Table 1. The sequences of gene-specific primers for reverse transcriptase–polymerase chain reaction (RT-PCR) and real-time RT-PCR used in this study

Primer	Sequence
IL-4 forward	CACAGGCACAAGCAGCTGAT
IL-4 reverse	CCTTCACAGGACAGGAATTCAAG
IL-6 forward	GTAGCCGCCCCACACAGA
IL-6 reverse	CCGTCGAGGATGTACCGAAT
IL-10 forward	GCCAAGCCTTGTCTGAGATGA
IL-10 reverse	CTTGATGTCTGGGTCTTGGTTCT
IL-17 forward	GACTCCTGGGAAGACCTCATTG
IL-17 reverse	TGTGATTCCTGCCTTCACTATGG
IL-17F forward	GCTTGACATTGGCATCATCAA
IL-17F reverse	GGAGCGGCTCTCGATGTTAC
IL-23 forward	GAGCCTTCTCTGCTCCCTGATAG
IL-23 reverse	AGTTGGCTGAGGCCCAGTAG
IL-23R forward	AACAACAGCTCGGCTTTGGTATA
IL-23R reverse	GGGACATTCAGCAGTGCAGTAC
IFNG forward	CATCCAAGTGATGGCTGAACTG
IFNG reverse	TCGAAACAGCATCTGACTCCTTT
GM-CSF forward	CAGCCCTGGAGCATGTG
GM-CSF reverse	CATCTCAGCAGCAGTGTCTCTAC^{r}
RORγt forward	TGGGCATGTCCCGAGATG
RORγt reverse	GCAGGCTGTCCCTCTGCTT
STAT-3 forward	GGAGGAGGCATTCGGAAAGT
STAT-3 reverse	GCGCTACCTGGGTCAGCTT
FOXP3 forward	GAGAAGCTGAGTGCCATGCA
FOXP3 reverse	GCCACAGATGAAGCCTTGGT

IL, interleukin; *IFNG*, interferon γ; *FOXP3*, forkhead box protein 3; *GM-CSF*, granulocyte–macrophage colony-stimulating factor; *RORγt*, retinoic acid receptor-related orphan receptor γ isoform t; *STAT*, signal transducer and activator of transcription.

transcribed and labelled using One-Cycle Target Labeling and Control Reagents as instructed by the manufacturer (Affymetrix, Santa Clara, CA). The labelled probes were hybridized to a Human Genome U133 Plus 2·0 Array (Affymetrix). The arrays were used in a single experiment and analysed with GENECHIP operating software 1.2 (Affymetrix). Background subtraction and normalization were performed using GENESPRING GX 7.3 software (Agilent Technologies, Santa Clara, CA). The signal intensity was pre-normalized based on the positive control genes (GAPDH and β-actin) for all measurements on that chip. To account for differences in detection efficiency between spots, the pre-normalized signal intensity of each gene was normalized to the median of pre-normalized measurements for that gene. The data were filtered as follows. (i) Genes that were scored as absent in all samples were eliminated. (ii) Genes with a signal intensity of < 90 were eliminated. (iii) Genes that exhibited increased (fold-change > 2) or decreased (fold-change > 2) expression in CB-derived $CD4^+$ T cells compared with PB-derived $CD4^+$ T cells were selected by comparing the mean value of signal intensities in each condition.

Immunofluorescence study

After periods of cultivation, cells were collected and stained with fluorescence-labelled monoclonal antibodies and analysed by flow cytometry (FC500; Beckman/Coulter, Fullerton, CA). A four-colour immunofluorescence study was performed with a combination of fluorescein isothiocyanate (FITC)-conjugated anti-CD3, phycoerythrin (PE)-conjugated anti- forkhead box protein 3 (Foxp3), phycoerythrin-cyanine-5 (PC5)-conjugated anti-CD4 and PC7-conjugated anti-CD8 (Beckman/Coulter). After staining of cell surface antigens, cells were permeabilized with IntraPrep (Dako, Glostrup, Denmark) and intracellular antigen (Foxp3) was further stained.

Statistical analysis

The statistical analysis was performed using a Student's *t*-test and a *P*-value < 0·05 was considered to be statistically significant.

Results

Expression profiles of activated $CD4^+$ T cells derived from human CB and PB

To compare the gene expression patterns of CB-derived $CD4^+$ cells and PB-derived $CD4^+$ cells, we performed DNA microarray analysis using the Affymetrix Human Genome U133 Plus 2·0 Array. After background subtraction, comparison of the gene expression profiles of two independent CB-derived $CD4^+$ samples and PB-derived $CD4^+$ samples was performed using a gene cluster analysis. The genes differentially expressed (fold-change > 2) between the activated $CD4^+$ T cells derived from CB and those derived from PB were selected, and 396 probes were found to exhibit higher levels of expression in CB-derived $CD4^+$ samples while 131 probes exhibited higher levels in PB-derived $CD4^+$ samples. Parts of the data are summarized and presented in Fig. 1a and Tables 2–4.

Among these genes, those closely correlated to T-cell function and development were selected (Fig. 1b). The genes exhibiting higher levels of expression in CB-derived $CD4^+$ samples included those encoding cell cycle regulators, including cyclin-dependent kinase (CDKN)2A and 2B, transcriptional regulators and signal transduction factors (Tables 2 and 3). The genes for cytokines, chemokines and their receptors such as Interferon γ (IFNG), granulocyte-macrophage colony-stimulating factor (GM-CSF) and for T-cell transcriptional regulators (*FOXP3*) as well as the genes related to T-cell development including CD28, cytotoxic T lymphocyte antigen-4 (CTLA4) and inducible T-cell co-stimulator (ICOS) were also found among the genes exhibiting higher levels of expression in CB-derived $CD4^+$ samples (Fig. 1b). The factors reported

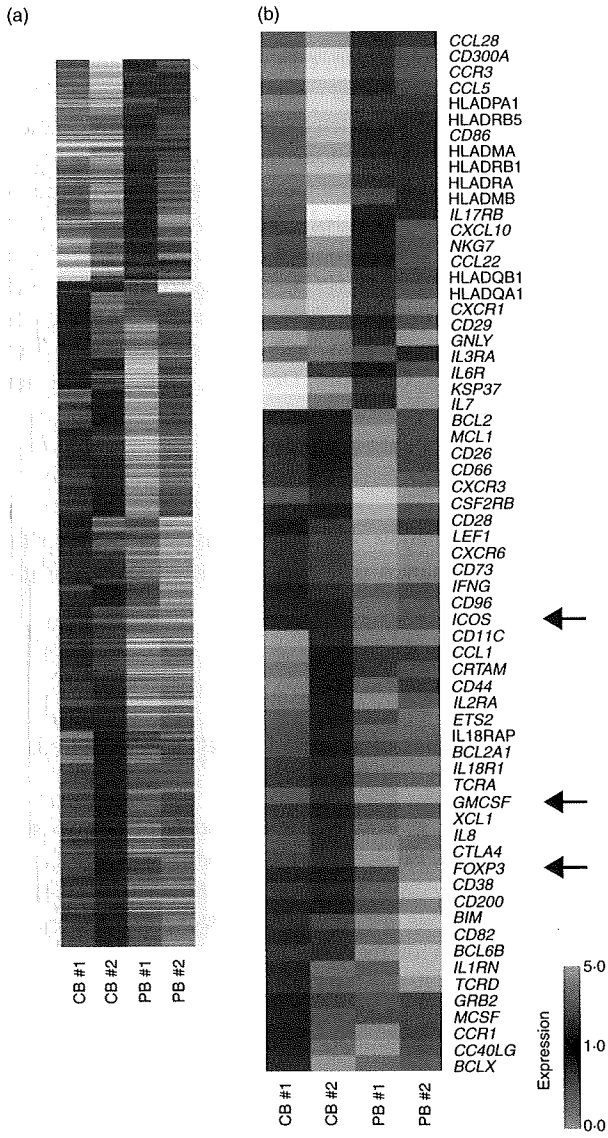

Figure 1. Comparison of the gene expression profiles of cord blood (CB)- and peripheral blood (PB)-derived $CD4^+$ T cells. Hierarchical clustering of results from a microarray analysis for CB- and PB-derived $CD4^+$ T cells is indicated. (a) A total of 529 genes characterizing $CD4^+$ T cells (396 genes for CB-derived $CD4^+$ T cells and 131 genes for PB-derived $CD4^+$ T cells) were used to create the gene tree. The gene list is presented in Tables 3 and 4. (b) Genes related to T-cell development (40 genes for CB-derived $CD4^+$ T cells and 26 genes for PB-derived $CD4^+$ T cells) are presented. The arrows indicate the expression pattern of T-cell lineage-specific genes including inducible T-cell co-stimulator (*ICOS*), granulocyte-macrophage colony-stimulating factor (*GM-CSF*) and forkhead box protein 3 (*FOXP3*).

to be essential for negative selection in $CD4^+$ $CD8^+$ thymocytes such as BCL2-like 11 (BIM)[10] as well as other apoptotic regulators were also found among the genes exhibiting higher expression levels in CB-derived $CD4^+$ samples.

The genes with a higher level of expression in the PB-derived $CD4^+$ T cells included those encoding transcriptional regulators, signal transduction factors, major histocompatibility complex (MHC) class II molecules (*HLADMA*, *HLADMB*, *HLADPA1*, *HLADQB1*, *HLADRA*, *HLADRB1* and *HLADRB5*), and cytokines, chemokines and their receptors (*IL-7*, *IL-17RB*), as well as genes that characterize the T-cell lineage (*CD29*, *CD86*) (Fig. 1b, Tables 2, 4).

Notably, microarray studies showed that the expression of several regulatory T cell (Treg)-related genes was significantly higher in the CB-derived T cells. Foxp3 is an important T-cell transcription factor and is considered to be a marker of Tregs. Cytotoxic T-lymphocyte antigen-4 (CTLA-4) and ICOS, which belong to the CD28 family of receptors and play a crucial role in the activation of T cells, were reported to be highly expressed in activated Tregs.[11,12] All of the above genes were expressed at higher levels in the CB-derived CD4 T cells (Fig. 1).

The microarray results for major genes related to the development of the T-cell lineage, including those not appeared in Fig. 1, are summarized in Table 2. As shown in Table 2, the expression of T-cell lineage master regulator genes, such as *TBX21*, *GATA3* and *MAF*, and T cell-related cytokines, such as *IL-4*, *IL-5*, *IL-13*, *IL-22* and *TGFB1*, revealed no significant difference between CB-derived $CD4^+$ cells and PB-derived $CD4^+$ cells. However, other T cell-related genes, including *IL-2*, *IL-6*, *IL-9*, *IL-10* and *IL-17*, were eliminated from the list in the course of background subtraction because the signal intensity of each gene was low (< 90 as raw data) in all of the samples.

Differences in the expression patterns of T-cell lineage-specific genes between CB-derived and PB-derived $CD4^+$ T cells

To further confirm the characteristic gene expression in CB- and PB-derived $CD4^+$ T cells, we performed a real-time RT-PCR analysis. Consistent with the microarray data, when the mRNA levels of the genes related to the T helper type 1 (Th1) and Th2 phenotypes were examined, higher levels of GM-CSF and IFNG were observed in CB-derived T cells, while IL-4 revealed no significant tendency (Fig. 2). We also examined IL-6 and IL-10 and no significant tendency was observed either in the expression of these genes (Fig. 2).

Next we examined the expression of the genes related to Tregs and observed a higher level of Foxp3, but lower levels of retinoic acid receptor-related orphan receptor γ isoform t (RORγt); and IL-17F, in CB-derived T cells (Fig. 3). In contrast, there was no significant tendency in the expression of genes encoding signal transducer and activator of transcription 3 (STAT-3), IL-23 and IL-23 receptors. In the case of the *IL-17* gene, clear amplifica-

Table 2. The microarray results for T-cell-related genes

Description	Gene	Gene ID	CB-I		CB-2		PB-1		PB-2	
			Normalized	Raw	Normalized	Raw	Normalized	Raw	Normalized	Raw
Master regulation										
Thl	*TBX21*	220684_at	1·1382915	305·7	0·7851455	247·1	1·045663	230·5	0·954337	261·4
Th2	*GATA3*	209602_s_at	1·471558	1204	0·7742825	742·1	1·0740323	721·1	0·9259675	772·5
	GATA3	209603_at	1·265932	416·5	0·53335179	205·7	1·0535141	284·5	0·9464856	317·6
	GATA3	209604_s_at	1·350573	5300	0·6415387	2950	1·0573606	3406	0·9426395	3773
	MAF	206363_at	0·7447395	672·7	0·8744312	925·6	1·1255689	834·5	1·2704437	1170
	MAF	209348_s_at	1·0320604	2078	0·8329663	1965	0·9679398	1600	1·8301903	3758
	MAF	229327_s_at	0·9099149	569·7	0·6089576	446·8	1·090085	560·2	1·4076804	898·9
Treg	*FOXP3*	221334_s_at	1·8893701	100·6	1·4199468	88·6	0·4988136	21·8	0·5800531	31·5
	FOXP3	224211_at	1·6205869	152·3	1·4101433	155·3	0·5898568	45·5	0·2347433	22·5
Cytokines										
Thl	*IFNG*	210354_at	1·4801383	2000	1·9182948	3037	0·457517	507·4	0·5198616	716·4
	GM-CSF	210229_s_at	1·2802086	1293	2·6726868	3163	0·6906437	572·5	0·7197912	741·4
Th2	*IL-4*	207538_at	2·0291064	687·2	0·3361219	133·4	0·9317174	259	1·0682826	369
	IL-4	207539_s_at	2·8263247	965	0·3561467	142·5	0·8481774	237·7	1·1518226	401·1
	IL-5	207952_at	1·3380713	810	0·0610382	43·3	1·0097023	501·7	0·9902797	611·4
	IL-13	207844_at	3·9835246	1712	0·8117443	408·8	1·1453367	404	0·8691162	452·9
Treg	*TGFB1*	203085_s_at	1·5166419	774·9	0·9012154	539·6	1·0987847	460·8	0·8546632	374·6
Others	*IL-22*	222974_at	0·1272062	5·2	4·325279	207·2	0·5632869	18·9	1·4367131	59·9
Surface molecules										
Treg	*CTLA4*	231794_at	1·3871489	336·9	1·2560804	357·5	0·7439196	148·3	0·4444751	110·1
	CTLA4	236341_at	1·2573498	905·7	1·6210791	1368	0·6800935	402·1	0·7426501	545·6
Others	*IL-2RA*	206341_at	1·5216751	3569	1·2715347	3494	0·7284654	1402	0·6569936	1571
	IL-2RA	211269_s_at	1·1563299	4436	1·3173387	5923	0·8436702	2657	0·560745	2194
	ICOS	210439_at	1·378036	619·8	1·343834	708·3	0·567216	209·4	0·656166	301
	CD28	211856_x_at	1·3887135	144·9	1·2905376	157·8	0·3292731	28·2	0·7094624	75·5
	CD28	211861_x_at	1·350062	183·3	1·4109998	224·5	0·4863549	54·2	0·649938	90

The microarray results for major genes related to the development of the T-cell lineage are summarized. The normalized and raw data for four samples are indicated for each gene. Those for which differential expression was found between cord blood (CB)- and peripheral blood (PB)-derived $CD4^+$ T cells in a gene cluster analysis (fold-change > 2) are highlighted in grey. Genes exhibiting low signal intensity (< 90 as raw data) in all of the four samples were eliminated from the list beforehand in the process of background subtraction, and thus do not appeared in this table.

CTLA-4, cytotoxic T-lymphocyte antigen-4; *FOXP3*, forkhead box protein 3; GATA, GATA family of zinc finger trancription factors; *GM-CSF*, granulocyte–macrophage colony-stimulating factor; ICOS, inducible T-cell co-stimulator; IFNG, interferon γ; *IL*, interleukin; MAF, macrophage-activating factor; TBX21, T-box protein 21; TGFB1, transforming growth factor, beta 1; Th1, T helper type 1; Treg, regulatory T cell.

tion was detected in PB-derived T cells whereas no amplification was observed in the samples of CB-derived T cells (data not shown).

To further investigate whether increased expression of the *FOXP3* gene is a general feature of CB-derived $CD4^+$ T cells, we tested four samples of CB-derived $CD4^+$ T cells by real-time RT-PCR analysis and compared the results with those for equivalent numbers of PB-derived samples. As shown in Fig. 4, two CB-derived samples (CB 4 and 5, at 2 weeks) revealed significantly increased gene expression of *FOXP3* when compared with PB-derived samples, whereas the remaining two samples (CB 3 and 6; termed 'additional' samples below) did not. We also tested *FOXP3* gene expression at an earlier time-point in the same samples and observed no significant increase of *FOXP3* gene expression in CB-derived $CD4^+$ T cells at 1 week (Fig. 4). When the data were analysed statistically, expression of the *FOXP3* gene was found to be significantly higher in CB-derived $CD4^+$ T cells in comparison with equivalent PB-derived $CD4^+$ T cells at both 1 week ($P < 0{\cdot}05$) and 2 weeks ($P < 0{\cdot}05$) (Fig. 4).

Next we assessed the expression of the Foxp3 protein in CB-derived $CD4^+$ T cells. When the same samples as described above were examined by flow cytometry using a specific antibody, the Foxp3 protein was certainly detected in a portion of cells in all of four CB-derived samples while not detected in any of the PB-derived samples tested (Fig. 5). Inconsistent with the results of real-time RT-PCR, expression level of Foxp3 proteins was higher in CB-derived $CD4^+$ T cells at 1 week than at 2 weeks.

Table 3. Genes up-regulated in $CD4^+$ T cells from cord blood samples 1 and 2 (CB 1 and CB 2, respectively)

Affi ID	Gene abbreviation	Fold change CB 1	CB 2	PB 1	PB 2	Gene name
Apoptosis						
1555372_at	*BimL*	1·39	1·52	0·61	0·42	BCL2-like 11 (apoptosis facilitator)
237837_at	*BCL2*	1·27	1·32	0·49	0·73	B-cell CLL/lymphoma 2
205681_at	*BCL2A1*	1·91	1·53	0·39	0·47	BCL2-related protein A1
1558143_a_at	*BCL2L11*	1·68	1·74	0·32	0·32	BGL2-like 11 (apoptosis facilitator)
228311_at	*BCL6B*	1·36	3·39	0·64	0·26	B-cell CLL/lymphoma 6, member B (zinc finger protein)
215037_s_at	*BCLX*	2·56	1·27	0·73	0·56	BCL2-like 1
224414_s_at	*CARD6*	2·65	1·34	0·56	0·66	Caspase recruitment domain family, member 6
201631_s_at	*IER3*	1·62	2·95	0·38	0·31	Immediate early response 3
218000_s_at	*PHLDA1*	2·34	1·21	0·53	0·79	Pleckstrin homology-like domain, family A, member 1
209803_s_at	*PHLDA2*	2·87	1·32	0·31	0·68	Pleckstrin homology-like domain, family A. member 2
203063_at	*PPMIF*	1·26	1·53	0·74	0·64	Protein phosphatase IF (PP2C domain containing)
205214_at	*STK17B*	1·78	1·26	0·74	0·71	Serine/threonine kinase 17b (apoptosis-inducing)
217853_at	*TENS1*	1·63	6·00	0·04	0·37	Tensin 1
B- and T-cell development						
211861_x_at	*CD28*	1·35	1·41	0·49	0·65	CD28 antigen(Tp44)
207892_at	*CD40LG*	3·67	1·32	0·45	0·68	C040 ligand (TNF superfamily, member 5, hyper-IgM syndrome)
206914_at	*CRTAM*	2·76	1·60	0·40	0·36	Class I MHC-restricted T-cell-associated molecule
210557_x_at	*CSF1*	3·79	1·22	0·78	0·70	Colony-stimulating factor 1 (macrophage)
210229_s_at	*CSF2*	1·28	2·67	0·69	0·72	Colony-stimulating factor 2 (granulocyte–macrophage)
205159_at	*CSF2RB*	2·33	1·60	0·18	0·40	Colony-stimulating factor 2 receptor
231794_at	*CTLA4*	1·39	1·26	0·74	0·44	Cytotoxic T-lymphocyte-associated protein 4
204232_at	*FCER1G*	1·63	2·14	0·28	0·37	Fc fragment of IgE, high affinity 1, receptor for; gamma polypeptide
210439_at	*ICOS*	1·38	1·34	0·57	0·66	Inducible T-cell costimulator
210354_at	*IFNG*	1·48	1·92	0·46	0·52	Human mRNA for HuIFN -gamma interferon
230536_at	*PBX4*	1·48	1·26	0·50	0·74	Pre-B-cell leukaemia transcription factor 4
215540_at	*TCRA*	1·25	1·87	0·67	0·75	T-cell antigen receptor alpha
234440_al	*TCRD*	7·51	1·48	0·50	0·52	Human T-cell receptor delta-chain
Cell growth and maintenance						
213497_at	*ABTB2*	2·06	1·34	0·66	0·63	Ankyrin repeat and BTB (POZ) domain containing 2
201236_s_at	*BTG2*	1·60	1·23	0·60	0·77	BTG family, member 2
235287_at	*CDK6*	1·50	1·32	0·44	0·68	Cyclin-dependent kinase 6
209644_x_at	*CDKN2A*	2·90	1·21	0·67	0·79	Cyclin-dependent kinase inhibitor 2A (melanoma, p16, inhibits CDK4)
236313_at	*CDKN2B*	3·24	1·28	0·58	0·72	Cyclin-dependent kinase inhibitor 2B (p15, inhibits CDK4)
241984_at	*CHES1*	1·38	1·34	0·66	0·63	Checkpoint suppressor 1
202552_s_at	CRIM1	1·94	1·39	0·32	0·61	Cysteine-rich transmembrane BMP regulator 1 (chordin-like)
204844_at	*ENPEP*	1·64	1·75	0·09	0·36	Glutamyl aminopeptidase (aminopeptidase A)
205418_at	*FES*	1·39	1·80	0·61	0·25	Feline sarcoma oncogene
228572_at	*GRB2*	4·69	1·21	0·79	0·78	Growth factor receptor-bound protein 2
207688_s_at	*INHBC*	1·46	1·25	0·51	0·75	Inhibin, beta C
209744_x_at	*ITCH*	1·30	1·47	0·63	0·70	Itchy homolog E3 ubiquitin protein ligase (mouse)
201548_s_at	*JARID1B*	1·27	1·92	0·73	0·46	Jumonji, AT-rich interactive domain IB (RBP2-like)
203297_s_at	*JARID2*	1·42	1·28	0·54	0·72	Jumonji, AT-rich interactive domain 2
41387_r_at	*JMJD3*	1·82	1·24	0·76	0·65	Jumonji domain containing 3
205569_at	*LAMP3*	2·32	1·24	0·76	0·50	Lysosomal-associated membrane protein 3
214039_s_at	*LAPTM4B*	1·41	1·49	0·49	0·59	Lysosomal-associated protein transmembrane 4 beta
205857_x_at	*MSH3*	1·79	1·28	0·58	0·72	MutS homolog 3 (*E. coli*)
209550_at	*NDN*	3·42	1·38	0·17	0·62	Necdin homolog (mouse)
207943_x_at	*PLAGL1*	1·37	1·43	0·57	0·63	Pleiomorphic adenoma gene-like 1
204748_at	*PTGS2*	1·65	1·78	0·14	0·35	Prostaglandin-endoperoxide synthase 2
201482_at	*QSCN6*	1·32	1·23	0·38	0·77	Quiescin Q6
203743_s_at	*TDG*	1·47	1·23	0·54	0·77	Thymine-DNA glycosylase
204227_s_at	*TK2*	2·12	1·26	0·56	0·74	Thymidine kinase 2, mitochondrial

Table 3. Continued

Affi ID	Gene abbreviation	Fold change CB 1	CB 2	PB 1	PB 2	Gene name
Cytokines and chemokines						
207533_at	*CCL1*	1·67	1·48	0·52	0·49	Chemokine (C-C motif) ligand 1
205099_s_at	*CCR1*	4·70	1·21	0·61	0·79	Chemokine (C-C motif) receptor 1
207681_at	*CXCR3*	1·51	1·33	0·41	0·67	Chemokine (C-X-C motif) receptor 3
211469_s_at	*CXCR6*	1·58	1·95	0·32	0·42	Chemokine (C-X-C motif) receptor 6
206613_at	*IL-18R1*	2·32	1·38	0·61	0·62	Interleukin-18 receptor 1
207072_at	*IL-18RAP*	2·16	1·44	0·46	0·56	Interleukin-18 receptor accessory protein
212657_s_at	*IL-1RN*	1·44	3·12	0·56	0·37	Interleukin 1 receptor
206341_at	*IL-2RA*	1·52	1·27	0·73	0·66	Interleukin-2 receptor alpha
202859_x_at	*IL-8*	1·31	3·75	0·38	0·69	Interleukin-8
202643_s_at	*TNFAIP3*	1·61	1·25	0·67	0·75	Tumour necrosis factor, alpha-induced protein 3
202687_s_at	*TNFSF10*	2·83	1·23	0·67	0·77	Tumour necrosis factor (ligand) superfamily member 10
205599_at	*TRAF1*	2·25	1·32	0·68	0·61	Tumour necrosis factor receptor-associated factor 1
202871_at	*TRAF4*	1·43	1·58	0·57	0·48	Tumour necrosis factor receptor-associated factor 4
206366_x_at	*XCL1*	1·24	2·66	0·46	0·76	Chemokine (C motif) ligand 1
Signal transduction						
210538_s_at	*AIP1*	1·35	1·54	0·65	0·61	Baculoviral IAP repeat-containing 3
209369_at	*ANXA3*	1·39	6·82	0·61	0·05	Annexin A3
1554343_a_at	*BRDG1*	1·45	1·67	0·52	0·55	BCR downstream signalling 1
225946_at	*C12orf2*	3·20	1·77	0·23	0·23	Ras association (RaIGDS/AF-6) domain family 8
204392_at	*CAMK1*	1·26	1·62	0·74	0·54	Calcium/calmodulin-dependent protein kinase I
231042_s_at	*CAMK2D*	1·31	1·63	0·25	0·69	Calcium/calmodulin-dependent protein kinase (CaM kinase) II delta
205692_s_at	*CD38*	1·37	1·29	0·71	0·48	CD38 antigen (p45)
231747_at	*CYSLTR1*	3·16	1·45	0·55	0·43	Cysteinyl leukotriene receptor 1
211272_s_at	*DGKA*	1·43	1·23	0·77	0·54	Diacylglycerol kinase alpha 80 kDa
200762_at	*DPYSL2*	1·35	1·40	0·37	0·65	Dihydropyrimtdinase-like 2
208370_s_at	*DSCR1*	1·23	1·90	0·63	0·77	Down syndrome critical region gene 1
204794_at	*DUSP2*	1·55	2·57	0·39	0·45	Dual specificity phosphatase 2
204015_s_at	*DUSP4*	1·35	2·66	0·65	0·39	Dual specificity phosphatase 4
211333_s_at	*FASLG*	1·20	1·37	0·49	0·80	Fas ligand (TNF superfamily, member 6)
211535_s_at	*FGFR1*	1·23	2·79	0·70	0·77	Fibroblast growth factor receptor 1
224148_at	*FYB*	1·50	1·21	0·45	0·79	FYN binding protein (FYB-120/130)
209304_x_at	*GADD45B*	1·55	1·29	0·65	0·71	Growth arrest and DNA-damage-inducible beta
234284_at	*GNG8*	1·50	3·16	0·50	0·35	Guanine nucleotide binding protein (G protein), gamma 8
224285_at	*GPR174*	1·91	1·42	0·56	0·58	G protein-coupled receptor 174
223767_at	*GPR84*	4·41	1·44	0·05	0·56	G protein-coupled receptor 84
211555_s_at	*GUCY1B3*	1·66	1·73	0·34	0·03	Guanylate cyclase 1, soluble, beta 3
38037_at	*HBEGF*	1·54	1·36	0·55	0·64	Heparin-binding EGF-like growth factor
203820_s_at	*IMP-3*	1·83	2·18	0·17	0·17	IGF-II-mRNA-binding protein 3
203006_at	*INPP5A*	1·40	1·86	0·60	0·52	Inositol polyphosphate-5-phosphatase, 40 kDa
231779_at	*IRAK2*	1·93	1·46	0·46	0·54	Interleukin-1 receptor associated kinase 2
32137_at	*JAG2*	1·58	1·29	0·71	0·64	Jagged 2
203904_x_at	*KAI1*	1·65	1·59	0·41	0·25	CD82 antigen
235252_at	*KSR*	1·72	1·56	0·43	0·44	Kinase suppressor of ras 1
210948_s_at	*LEF1*	1·21	1·64	0·41	0·79	Hypothetical protein LOC641518
203236_s_at	*LGALS9*	1·48	1·27	0·73	0·51	Lectin, galactoside-binding, soluble, 9 (galectin 9)
220253_s_at	*LRP12*	1·27	1·30	0·31	0·73	Low-density lipoprotein-related protein 12
206637_at	*P2RY14*	1·32	1·48	0·39	0·68	Purinergic receptor P2Y, G-protein coupled, 14
210837_s_at	*PDE4D*	1·35	1·31	0·62	0·69	Phosphodiesterase 4D, cAMP-specific
206726_at	*PGDS*	6·45	1·40	0·60	0·43	Prostaglandin D2 synthase, haematopoietic
210617_at	*PHEX*	1·53	4·08	0·21	0·47	Phosphate regulating endopeptidase homologue, X-linked
206370_at	*PIK3CG*	1·23	1·32	0·50	0·77	Phosphoinositide-3-kinase, catalytic, gamma polypeptide
205632_s_at	*PIP5K1B*	1·32	1·42	0·64	0·68	Phosphalidylinositol-4-phosphate 5-kinase, type 1 beta

Table 3. Continued

Affi ID	Gene abbreviation	Fold change CB 1	CB 2	PB 1	PB 2	Gene name
215195_at	*PRKCA*	2·17	1·36	0·64	0·61	Protein kinase C, alpha
210832_x_at	*PTGER3*	4·44	1·47	0·07	0·53	Prostaglandin E receptor 3 (subtype EP3)
1553535_a_at	*RANGAP1*	1·58	1·39	0·58	0·61	Ran GTPase activating protein 1
234344_at	*RAP2C*	1·75	1·26	0·46	0·74	RAP2C, member of RAS oncogene family
223809_at	*RGS18*	2·12	1·67	0·15	0·33	Regulator of G-protein signalling 18
209882_at	*RIT1*	1·74	1·32	0·63	0·68	Ras-like without CAAX 1
209451_at	*TANK*	1·34	1·20	0·42	0·80	TRAF family member-associated NFKB activator
204924_at	*TLR2*	1·60	2·52	0·36	0·40	Toll-like receptor 2
217979_at	*TM4SF13*	1·21	2·47	0·30	0·79	Tetraspanin 13
209263_x_at	*TM4SF7*	2·05	1·41	0·58	0·59	Tetraspanin 4
Transcription						
1566989_at	*ARID1B*	1·42	1·27	0·09	0·73	AT-rich interactive domain 1B (SWIl-like)
203973_s_at	*CEBPD*	3·06	1·51	0·33	0·49	CCAAT/enhancer binding protein (C/EBP), delta
221598_s_at	*CRSP8*	1·60	1·29	0·71	0·68	Cofactor required for Spl transcriptional activation, subunit 8, 34 kDa
205249_at	*EGR2*	1·33	4·27	0·67	0·60	Early growth response 2 (Krox-20 homologue, *Drosophila*)
206115_at	*EGR3*	1·31	6·15	0·69	0·48	Early growth response 3
201328_at	*ETS2*	1·57	1·72	0·43	0·40	V-ets erythroblastosis virus E26 oncogene homologue 2 (avian)
218810_at	*FLJ23231*	2·13	1·37	0·63	0·63	Zinc finger CCCH-type containing 12A
209189_at	*FOS*	21·56	1·31	0·13	0·69	V-fos FBJ murine osteosarcoma viral oncogene homologue
223408_s_at	*FOXK2*	2·26	1·22	0·48	0·78	Forkhead box K2
202723_s_at	*FOXO1A*	1·47	1·27	0·57	0·73	Forkhead box O1A (rhabdomyosarcoma)
224211_at	*FOXP3*	1·62	1·41	0·59	0·23	Forkhead box P3
207156_at	*HIST1H2AG*	1·73	1·30	0·41	0·70	Histone 1, H2ag
220042_x_at	*HIVEP3*	1·26	1·65	0·74	0·56	Human immunodeficiency virus type I enhancer binding protein 3
207826_s_at	*ID3*	1·34	8·64	0·60	0·66	Inhibitor of DNA binding 3, dominant negative helix-loop-hetix protein
204549_at	*IKBKE*	2·33	1·29	0·71	0·66	Inhibitor of kappa light polypeptide gene enhancer in B cells
219878_s_at	*KLF13*	1·89	1·26	0·34	0·74	Kruppel-like factor 13
207667_s_at	*MAP2K3*	1·33	1·28	0·72	0·57	Mitogen-activated protein kinase kinase 3
201502_s_at	*NFKBIA*	2·31	1·29	0·71	0·57	Nuclear factor of κ light polypeptide gene enhancer in B cells inhibitor
222105_s_at	*NKIRAS2*	1·84	1·21	0·69	0·79	NFKB inhibitor interacting Ras-like 2
204622_x_at	*NR4A2*	1·35	4·31	0·65	0·63	Nuclear receptor subfamily 4, group A, member 2
207978_s_at	*NR4A3*	1·33	3·53	0·62	0·67	Nuclear receptor subfamily 4, group A, member 3
202600_s_at	*NRIPI*	1·86	1·39	0·26	0·61	Nuclear receptor interacting protein 1
216841_s_at	*SOD2*	1·25	1·73	0·36	0·75	Superoxide dismutase 2, mitochondrial
201416_at	*SOX4*	1·53	2·21	0·47	0·38	SRY (sex determining region Y)-box 4
223635_s_at	*SSBP3*	2·12	1·25	0·75	0·62	Single-stranded DNA binding protein 3
206506_s_at	*SUPT3H*	1·47	1·31	0·57	0·69	Suppressor of Ty 3 homologue (*S. cerevisiae*)
221618_s_at	*TAF9L*	1·25	1·49	0·47	0·75	TAF9-like RNA polymerase II
203177_x_at	*TFAM*	1·63	1·23	0·77	0·57	Transcription factor A, mitochondrial
213943_at	*TWIST1*	1·89	3·14	0·04	0·11	Twist homologue 1 (acrocephalosyndactyly 3; Saethre-Chotzen syndrome)
219836_at	*ZBED2*	1·33	4·76	0·67	0·21	Zinc finger, BED-type containing 2
211965_at	*ZFP36L1*	2·02	1·47	0·29	0·53	Zinc finger protein 36, C3H type-like 1
230760_at	*ZFY*	1·41	1·25	0·75	0·02	Zinc finger protein, Y-linked
228854_at	*ZNF145*	3·26	1·21	0·40	0·79	Transcribed locus
235121_at	*ZNF542*	2·68	1·33	0·63	0·67	Zinc finger protein 542

To investigate whether increased expression of the *IL-17* gene is a general feature of PB-derived $CD4^+$ T cells, we also tested *IL-17* gene expression in the above-described additional samples by real-time RT-PCR analysis. As shown in Fig. 6, all of four PB-derived $CD4^+$ T-cell samples revealed significantly increased gene expression of *IL-17* when compared with the CB-derived samples at 1 week. At 2 weeks, however, *IL-17* gene expression in PB-derived $CD4^+$ T cells was diminished while some of the CB-derived $CD4^+$ T cells (such as sample CB 4) exhibited increased *IL-17* gene expression. When the data were analysed statistically, expression of the *IL-17* gene was found to be

Table 4. Genes up-regulated in $CD4^+$ T cells from peripheral blood (PB)

Affi ID	Gene abbreviation	Fold change CB 1	CB 2	PB 1	PB 2	Gene name
Apoptosis						
1553681_a_at	*PRF1*	0·66	0·51	1·41	1·34	Perforin 1 (pore-forming protein)
B- and T-cell development						
224499_s_at	*AICDA*	0·06	0·44	1·56	3·47	Activation-induced cytidine deaminase
205495_s_at	*GNLY*	0·40	0·51	1·49	6·34	Granulysin
217478_s_at	*HLA-DMA*	0·67	0·39	1·33	1·35	Major histocompatibility complex, class II, DM alpha
203932_at	*HLA-DMB*	0·64	0·31	2·02	1·36	Major histocompatibility complex, class II, DM beta
211991_s_at	*HLA-DPA1*	0·50	0·14	1·54	1·50	Major histocompatibility complex, class II, DP alpha 1
212671_s_at	*HLA-DQA1*	0·44	0·23	1·56	2·56	Major histocompatibility complex, class II, DQ alpha 1
211656_x_at	*HLA-DQB1*	0·63	0·48	1·37	7·07	Major histocompatibility complex, class II, DQ beta 1
210982_s_at	*HLA-DRA*	0·58	0·37	1·50	1·42	Major histocompatibility complex, class II, DR alpha
208306_x_at	*HLA-DRB1*	0·51	0·24	1·49	1·61	Major histocompatibility complex, class II, DR beta 3
204670_x_at	*HLA-DRB5*	0·63	0·22	1·47	1·37	Major histocompatibility complex, class II, DR beta 5
211634_x_at	*IGHV1-69*	0·69	0·77	1·23	1·99	Immunoglobulin heavy variable 1–69
211645_x_at	*IgK*	0·15	0·49	1·51	6·62	Immunoglobulin kappa light chain (IGKV)
221651_x_at	*IGKC*	0·46	0·68	1·32	5·57	Immunoglobulin kappa constant
215379_x_at	*IGLC2*	0·62	0·41	1·38	4·26	Immunoglobulin lambda joining 2
209031_at	*IGSF4*	0·50	0·03	2·33	1·50	Immunoglobulin superfamily, member 4
205686_s_at	*CD86*	0·70	0·23	1·30	1·39	CD86 antigen (CD28 antigen ligand 2, B7-2 antigen)
204698_at	*ISG20*	0·68	0·49	1·32	1·64	Interferon stimulated exonuclease gene, 20 kDa
213915_at	*NKG7*	0·72	0·42	1·28	2·31	Natural killer cell group 7 sequence
Cell growth and maintenance						
201334_s_at	*ARHGEF12*	0·74	0·50	1·26	1·96	Rho guanine nucleotide exchange factor (GEF) 12
230292_at	*CHC1L*	0·70	0·56	1·30	2·02	Regulator of chromosome condensation (RCC1)
205081_at	*CRIP1*	0·56	0·73	1·27	1·75	Cysteine-rich protein 1 (intestinal)
31874_at	*GAS2L1*	0·77	0·52	1·23	2·35	Growth arrest-specific 2 like 1
202364_at	*MXI1*	0·43	0·73	1·27	1·44	MAX interactor 1
219304_s_at	*PDGFD*	0·65	0·71	1·29	3·68	Platelet-derived growth factor D
213397_x_at	*RNASE4*	0·64	0·46	1·36	2·21	Ribonuclease, RNase A family, 4
213566_at	*RNASE6*	0·69	0·39	1·49	1·31	Ribonuclease, RNase A family, k6
219077_s_at	*WWOX*	0·40	0·78	1·25	1·22	WW domain containing oxidoreductase
Cytokine and chemokine						
207861_at	*CCL22*	0·76	0·52	1·24	2·47	Chemokine (C–C motif) ligand 22
238750_at	*CCL28*	0·74	0·45	1·26	1·41	Chemokine (C–C motif) ligand 28
1555759_a_at	*CCL5*	0·71	0·23	1·29	1·92	Chemokine (C–C motif) ligand 5
208304_at	*CCR3*	0·50	0·12	1·50	2·35	Chemokine (C–C motif) receptor 3
205898_at	*CX3CR1*	0·30	0·20	1·70	4·16	Chemokine (C–X3–C motif) receptor 1
204533_at	*CXCL10*	0·80	0·16	1·20	2·53	Chemokine (C–X–C motif) ligand 10
219255_x_at	*IL-17RB*	0·73	0·04	1·27	1·29	Interleukin 17 receptor B
206148_at	*IL-3RA*	0·60	0·54	2·46	1·40	Interleukin 3 receptor, alpha (low affnity)
226333_at	*IL-6R*	0·22	0·79	1·21	2·43	Interleukin-6 receptor
206693_at	*IL-7*	0·09	0·54	1·46	5·86	Interleukin-7
Signal transduction						
204497_at	*ADCY9*	0·76	0·40	1·24	2·40	Adenylate cyclase 9
206170_at	*ADRB2*	0·58	0·35	1·42	3·97	Adrenergic, beta-2-, receptor, surface
202096_s_at	*BZRP*	0·50	0·54	1·59	1·46	Benzodiazapine receptor (peripheral)
230464_at	*EDG8*	0·04	0·09	1·91	2·42	Endothelial differentiation, sphingolipid G-protein-coupled receptor 8
223423_at	*GPR160*	0·54	0·68	1·40	1·32	G protein-coupled receptor 160
227769_at	*GPR27*	0·07	0·08	1·92	244	G protein in-coupled receptor 27
210095_s_at	*IGFBP3*	0·27	0·20	1·73	5·25	Insulin-like growth factor binding protein 3
38671_at	*PLXND1*	0·08	0·65	1·35	2·57	Plexin D1
226101_at	*PRKCE*	0·56	0·43	1·72	1·44	Protein kinase C. epsilon
232629_at	*PROK2*	0·01	0·13	1·87	2·09	Prokineticin 2

Table 4. Continued

Affi ID	Gene abbreviation	Fold change CB 1	CB 2	PB 1	PB 2	Gene name
203329_at	*PTPRM*	0·36	0·62	1·38	1·93	Protein tyrosine phosphatase, receptor type, M
204731_at	*TGFBR3*	0·78	0·55	1·22	2·04	Transforming growth factor, beta receptor III (betaglycan, 300 kDa)
Transcription						
203129_s_at	*KIF5C*	0·67	0·09	1·33	3·43	Kinesin family member 5C
213906_at	*MYBL1*	0·75	0·51	1·25	3·63	V-myb myeloblastosis viral oncogene homologue (avian)-like 1
209815_at	*PTCH*	0·59	0·27	1·41	4·17	Patched homologue (*Drosophila*)
213891_s_at	*TCF4*	0·74	0·65	2·06	1·26	Transcription factor 4
238520_at	*TRERFI*	0·70	0·77	1·23	2·30	Transcriptional regulating factor 1
203603_s_at	*ZFHX1B*	0·74	0·61	1·26	3·63	Zinc finger homobox 1b
213218_at	*ZNF187*	0·74	0·69	1·26	1·76	Zinc finger protein 187
221123_x_at	*ZNF395*	0·38	0·71	1·63	1·29	Zinc finger protein 395

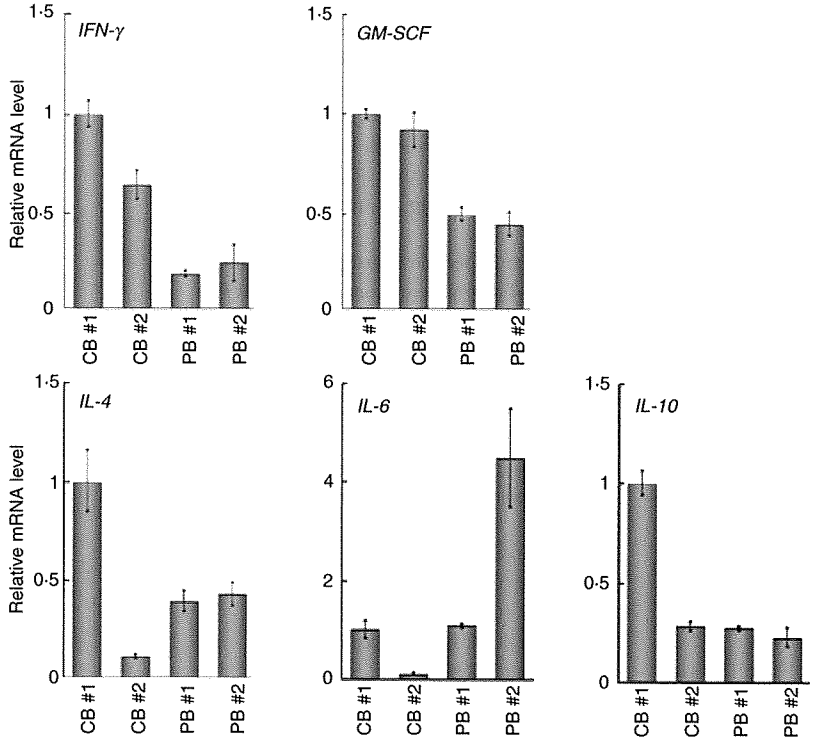

Figure 2. Quantitative polymerase chain reaction (PCR) analysis of the genes related to the T helper type 1 (Th1) and Th2 phenotypes. The expression of the genes indicated was examined by real-time reverse transcriptase (RT)-PCR using the same sample specimens as in Fig 1. Data are normalized to the mRNA level in PB 1 which is arbitrarily set to 1. The signal intensity was normalized using that of a control housekeeping gene [the human glyceraldehyde-3-phosphate dehydrogenase (*GAPDH*) gene]. Data are relative values with the standard deviation (SD) for triplicate wells.

significantly higher in PB-derived $CD4^+$ T cells in comparison with equivalent CB-derived $CD4^+$ T cells at 1 week ($P < 0·05$) but not at 2 weeks (Fig. 6).

Discussion

Although it is generally believed that there are functional differences between CB and PB lymphocytes, the details are obscure. For instance, Azuma *et al.*[13] reported that the phenotype and function of expanded CB lymphocytes were essentially equivalent to those of expanded PB lymphocytes when evaluated in *in vitro* experiments. In the present study, however, we have shown that CB-derived $CD4^+$ T cells revealed a distinct expression profile of genes important for the function of particular T-cell subsets compared with PB-derived $CD4^+$ T cells.

$CD4^+$ T cells can be classified into distinct subsets, including effector $CD4^+$ cells and Tregs, according to their functional characteristics as well as differentiation profiles.[14–16] Typically, effector $CD4^+$ T cells have been further divided into two distinct lineages on the basis of their cytokine production profiles, namely Th1 and Th2. Th1 cells producing cytokines such as IL-2, IFN-γ and GM-CSF have evolved to enhance the eradication of intracellular pathogens and are thought to be potent activators of cell-mediated immunity. In contrast, Th2

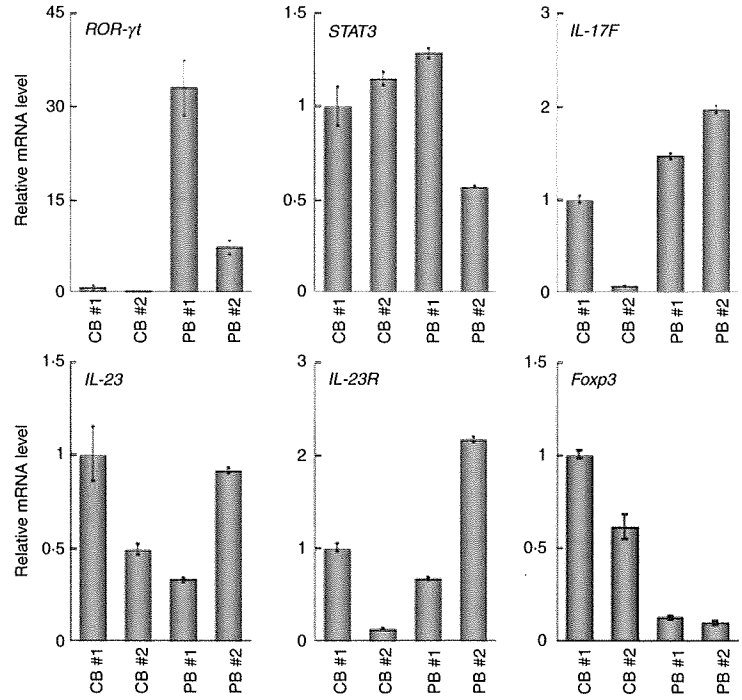

Figure 3. Quantitative polymerase chain reaction (PCR) analysis of the forkhead box protein 3 gene (*FOXP3*) and the genes related to the secretion of interleukin (IL)-17. The expression of the genes indicated was examined as in Fig 2. Data are normalized to the mRNA level in peripheral blood sample 1 (PB 1) as in Fig.2. The signal intensity was normalized using that of a control housekeeping gene [the human glyceraldehyde-3-phosphate dehydrogenase (*GAPDH*) gene]. Data are relative values with the standard deviation for triplicate wells.

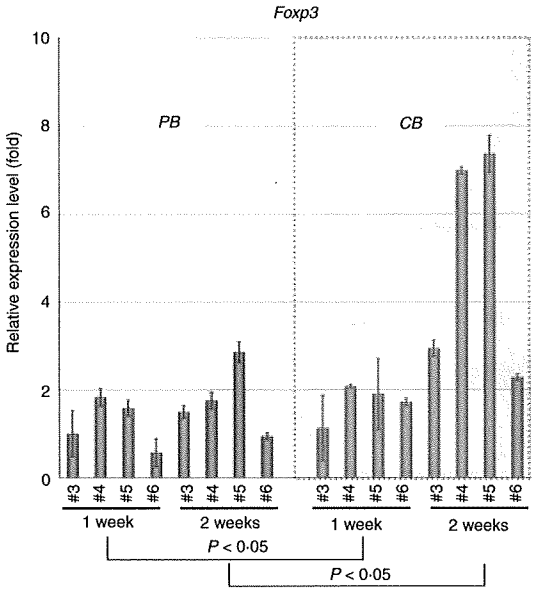

Figure 4. Quantitative polymerase chain reaction (PCR) analysis of the forkhead box protein 3 gene (*FOXP3*) in additional samples. Additional peripheral blood (PB) and cord blood (CB) samples were prepared and RNAs were extracted at 1 and 2 weeks. The expression of the *FOXP3* gene was examined as in Fig. 2. Data are normalized to the mRNA level in the sample of PB 3 at 1 week, which is arbitrarily set to 1. The signal intensity was normalized using that of a control housekeeping gene (the human β-actin gene). Data are relative values with the standard deviation for triplicate wells. The data were analysed statistically and *FOXP3* gene expression in CB-derived $CD4^+$ T cells was found to be significantly higher in comparison with equivalent PB-derived $CD4^+$ T cells at both 1 week ($P < 0{\cdot}05$) and 2 weeks ($P < 0{\cdot}05$).

cells secreting cytokines such as IL-4, IL-5, IL-6, IL-9 and IL-13 have evolved to enhance the elimination of parasitic infections and are thought to be potent activators of B-cell immunoglobulin E production, eosinophil recruitment, and mucosal expulsion. Th1-type responses to self or commensal floral antigens can promote tissue destruction and chronic inflammation, whereas dysregulated Th2-type responses can cause allergy and asthma. The development of Th1 is specified by the transcription factor T-bet (also known as Tbx-21) and master regulators of Th2 differentiation are GATA-3 and c-maf.

As shown in Fig. 2 and Table 2, the gene expression profiles of CB- and PB-derived $CD4^+$ T cells revealed no significant differences regarding cytokines related to the definition of Th1 and Th2, with the exceptions of IFN-γ and GM-CSF. The mRNA levels of IFN-γ and GM-CSF tended to be higher in CB-derived $CD4^+$ T cells than in PB-derived $CD4^+$ T cells. The mRNA expression of the transcription factors T-bet, GATA-3 and c-maf, which regulate Th1 and Th2 cell differentiation, did not differ significantly between CB- and PB-derived $CD4^+$ T cells.

In addition to Th1 and Th2 cells, IL-17 (also known as IL-17A)-producing T lymphocytes have been recently shown to comprise a distinct third subset of T helper cells, termed Th17 cells, in the mouse immune system. Th17 cells exhibit pro-inflammatory characteristics and act as major contributors to autoimmune disease. A number of experiments using animal models support a significant role for IL-17 in the response to allografts.[14,16,17] There is as yet no direct evidence for the existence of discrete Th17 cells in humans, although

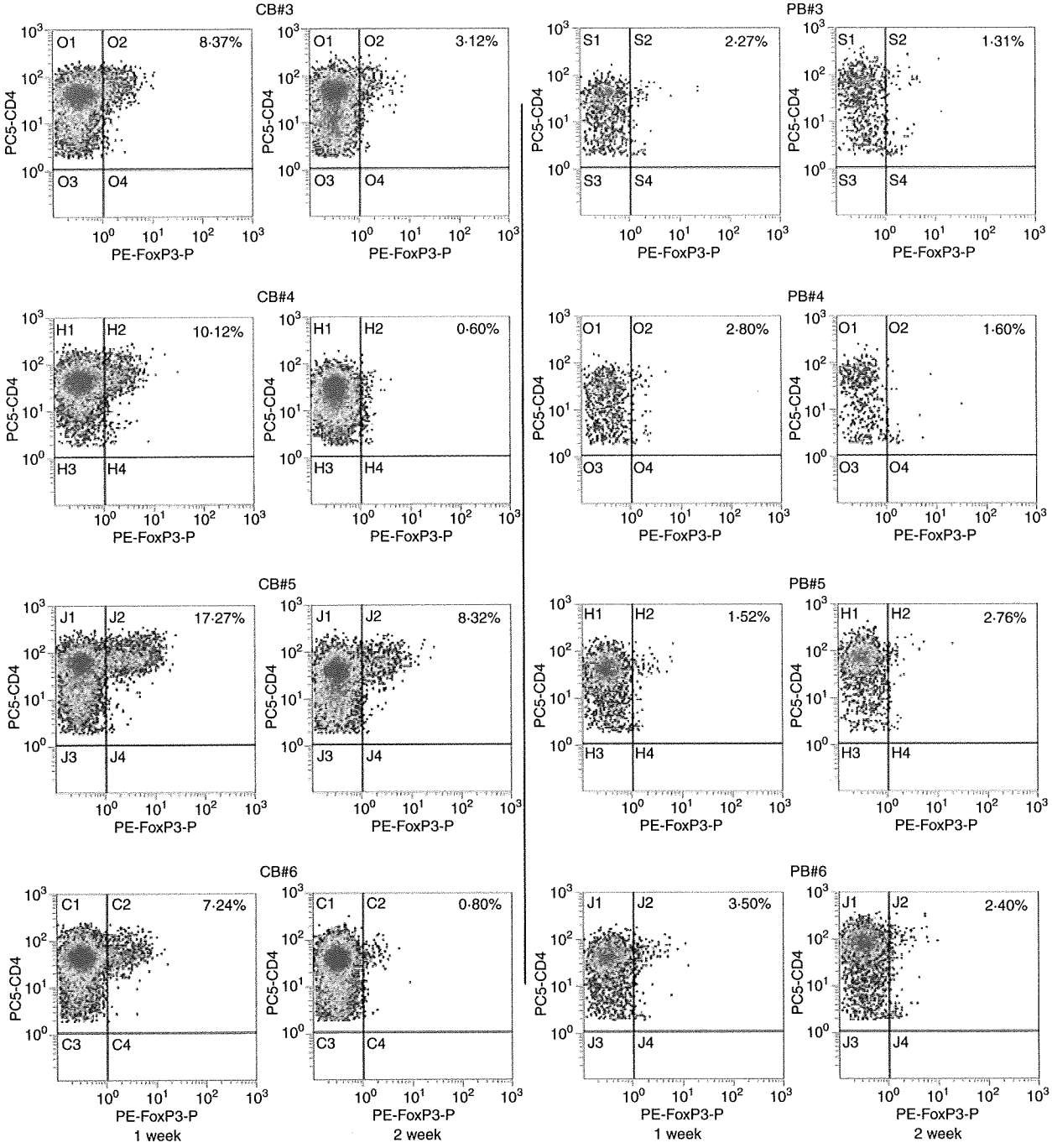

Figure 5. Protein expression of forkhead box protein 3 (Foxp3) in activated $CD4^+$ T cells. The protein expression of Foxp3 in same sample specimens as in Fig. 4 was examined by flow cytometry. The CD4 versus Foxp3 cytogram of the population gated with $CD3^+$ and $CD4^+$ in each sample is presented.

helper T cells secreting IL-17 have clearly been detected in the human immune system.[18] Several studies have shown a correlation between allograft rejection and IL-17. For example, IL-17 levels are elevated in human renal allografts during subclinical rejection and there are detectable mRNA levels in the urinary mononuclear cell sediments of these patients.[19,20] In human lung organ transplantation, IL-17 levels have also been reported to be elevated during acute rejection.[21] Interestingly, in this study, most of the PB-derived $CD4^+$ T-cell samples expressed higher levels of IL-17 mRNA than the CB-derived $CD4^+$ T-cell samples, suggesting that PB-derived $CD4^+$ T cells frequently include potent IL-17-secreting T cells.

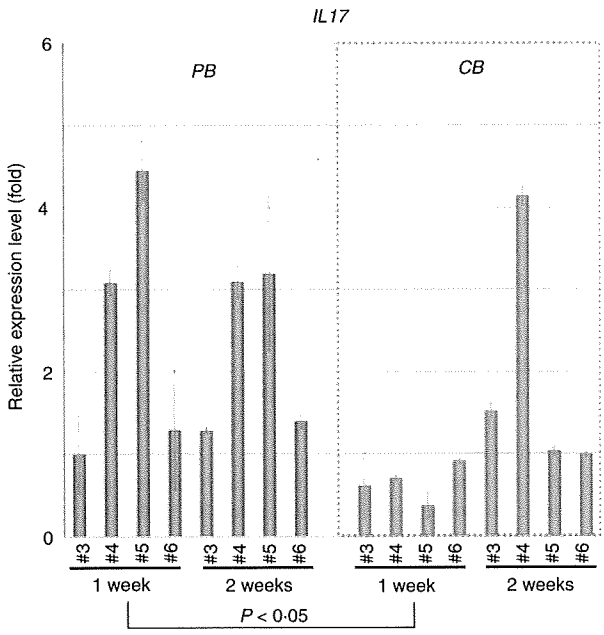

Figure 6. Quantitative polymerase chain reaction (PCR) analysis of interleukin (IL)-17 in additional samples. The expression of the *IL-17* gene in the same sample specimens as in Fig. 4 was examined and presented as in Fig 2. The data were analysed statistically and *IL-17* gene expression in peripheral blood (PB)-derived $CD4^+$ T cells was found to be significantly higher in comparison with equivalent CB-derived $CD4^+$ T cells at 1 week ($P < 0{\cdot}05$) but not at 2 weeks.

Th17 cells expand independently of T-bet or STAT-1. Ivanov *et al.*[22] have shown that the orphan nuclear receptor RORγt is the key transcription factor orchestrating the differentiation of the effector lineage. RORγt induces transcription of the gene encoding IL-17 in naïve $CD4^+$ T helper cells and is required for its expression in response to IL-6 and transforming growth factor (TGF)-β, the cytokines known to induce IL-17 expression. IL-23 is also involved in Th17 cell differentiation, but naïve T cells do not have the IL-23 receptor and are relatively refractory to IL-23 stimulation.[23,24] Although IL-23 seems to be an essential survival factor for Th17 cells, it is not required during their differentiation. It has been suggested that IL-23R expression is up-regulated on $ROR\gamma t^+$ Th17 cells in an IL-6-dependent manner. IL-23 may therefore function subsequent to IL-6/TGF-β-induced commitment to the Th17 lineage to promote cell survival and expansion and, potentially, the continued expression of IL-17 and other cytokines that characterize the Th17 phenotype. As presented in Fig. 3, the expression of the *RORγt* gene was significantly weaker in CB-derived $CD4^+$ T cells, whereas the expression of genes encoding IL-23 and the IL-23 receptor did not differ significantly between the $CD4^+$ T cells. Based on the above findings of others, it is possible that the low-level expression of the *RORγt* gene in CB-derived $CD4^+$ T cells is responsible for the absence of *IL-17* mRNA expression in those cells.

Tregs are another functional subset of T cells having anti-inflammatory properties and can cause quiescence of autoimmune diseases and prolongation of transplant function. *In vitro*, Tregs have the ability to inhibit the proliferation and production of cytokines by responder ($CD4^+$ $CD25^-$ and $CD8^+$) T cells subjected to polyclonal stimuli, as well as to down-regulate the responses of $CD8^+$ T cells, NK cells and $CD4^+$ cells to specific antigens.[25,26] These predicates translate *in vivo* to a great number of functions other than the maintenance of tolerance to self-components (prevention of autoimmune disease), such as the ability to prevent transplant rejection. Indeed, donor-specific Tregs can prevent allograft rejection in some models of murine transplant tolerance through a predominant effect on indirect alloresponses.

Foxp3 is thought to be responsible for the development of the Treg population and can act as a phenotypic marker of this fraction.[27] Tregs constitutively express CTLA-4 and there are suggestions that signalling through this pathway may be important for their function, as antibodies to CTLA-4 can inhibit Treg-mediated suppression.[28] As shown above, most of the CB-derived $CD4^+$ T cells were found to express either the *FOXP3* gene or the Foxp3 protein at higher levels compared with PB-derived $CD4^+$ T cells, suggesting that CB-derived $CD4^+$ T cells frequently include a potent Treg population.

As described above, *IL-17* mRNA was more detectable in PB-derived $CD4^+$ cells while *FOXP3* mRNA expression was higher in CB-derived $CD4^+$ cells. Post-transcriptional regulation, as well as differences in mRNA and protein turnover rates, can cause discrepancies between mRNA and protein expression and thus the differences observed in the mRNA expression do not necessary directly indicate those in protein expression.[29] Indeed, we observed some discrepancy between the levels of mRNA and protein with regard to Foxp3 expression in CB-derived $CD4^+$ T cells, as presented above. Nevertheless, changes in mRNA expression are mediated by the alteration of transcriptional regulation, and thus should indicate the differentiation ability of the cells. Therefore, our data indicate that CB-derived $CD4^+$ T cells tend frequently to include potent Tregs, while PB-derived $CD4^+$ T cells tend to include potent IL-17-secreting cells. As described above, DLI with donor CB-derived activated $CD4^+$ T cells is currently becoming established as a routine therapeutic strategy in Japan. It has been proposed that the skewing of responses towards Th17 or Th1 cells and away from Tregs may be responsible for the development and/or progression of autoimmune diseases or acute transplant rejection, and it may thus also be speculated that CB-derived $CD4^+$ T cells are more appropriate for DLI than PB-derived $CD4^+$ T cells.

However, our data also indicate the presence of individual, donor-dependent variations in the characteristics of activated $CD4^+$ T cells derived from CB and PB. More-

over, activated $CD4^+$ T cells do not consist of a single population and should include several distinct functional subsets of $CD4^+$ T cells. Therefore, it is important to clarify the characteristics of activated $CD4^+$ T cells in each preparation to predict the therapeutic effect of DLI in each clinical case.

In summary, our findings demonstrate a difference in gene expression between activated $CD4^+$ T cells derived from CB and those derived from PB. The higher level of *FOXP3* gene expression and the lower level of *IL-17* gene expression in CB-derived $CD4^+$ T cells may indicate that these cells have potential as immunomodulators in DLI therapy. Further detailed analysis should reveal the advantages of activated $CD4^+$ T cells from CB in DLI.

Acknowledgements

We thank the Tokyo Cord Blood Bank for the distribution of cord blood for research use. This work was supported by a grant from the Japan Health Sciences Foundation for Research on Publicly Essential Drugs and Medical Devices (KHC2032), Health and Labour Sciences Research Grants (the 3rd term comprehensive 10-year strategy for cancer control H19-010, Research on Children and Families H18-005, Research on Human Genome Tailor-made and Research on Publicly Essential Drugs and Medical Devices H18-005), and a Grant for Child Health and Development from the Ministry of Health, Labour and Welfare of Japan. It was also supported by CREST, JST.

Disclosures

No competing personal or financial interests exist for any of the authors in relation to this manuscript.

References

1 Loren AW, Porter DL. Donor leukocyte infusions after unrelated donor hematopoietic stem cell transplantation. *Curr Opin Oncol* 2006; **18**:107–14.
2 Roush KS, Hillyer CD. Donor lymphocyte infusion therapy. *Transfus Med Rev* 2002; **16**:161–76.
3 Alyea EP, Soiffer RJ, Canning C *et al.* Toxicity and efficacy of defined doses of CD4(+) donor lymphocytes for treatment of relapse after allogeneic bone marrow transplant. *Blood* 1998; **91**:3671–80.
4 Giralt S, Hester J, Huh Y *et al.* CD8-depleted donor lymphocyte infusion as treatment for relapsed chronic myelogenous leukemia after allogeneic bone marrow transplantation. *Blood* 1995; **86**:4337–43.
5 Tomizawa D, Aoki Y, Nagasawa M *et al.* Novel adopted immunotherapy for mixed chimerism after unrelated cord blood transplantation in Omenn syndrome. *Eur J Haematol* 2005; **75**:441–4.
6 Cohena Y, Nagler A. Hematopoietic stem-cell transplantation using umbilical-cord blood. *Leuk Lymphoma* 2003; **44**:1287–99.
7 Parmar S, Robinson SN, Komanduri K *et al.* Ex vivo expanded umbilical cord blood T cells maintain naive phenotype and TCR diversity. *Cytotherapy* 2006; **8**:149–57.
8 Robinson KL, Ayello J, Hughes R, van de Ven C, Issitt L, Kurtzberg J, Cairo MS. Ex vivo expansion, maturation, and activation of umbilical cord blood-derived T lymphocytes with IL-2, IL-12, anti-CD3, and IL-7. Potential for adoptive cellular immunotherapy post-umbilical cord blood transplantation. *Exp Hematol* 2002; **30**:245–51.
9 Miyagawa Y, Okita H, Nakaijima H *et al.* Inducible expression of chimeric EWS/ETS proteins confers Ewing's family tumor-like phenotypes to human mesenchymal progenitor cells. *Mol Cell Biol* 2008; **28**:2125–37.
10 Werlen G, Hausmann B, Naeher D, Palmer E. Signaling life and death in the thymus: timing is everything. *Science* 2003; **299**:1859–63.
11 Riley JL, June CH. The CD28 family: a T-cell rheostat for therapeutic control of T-cell activation. *Blood* 2005; **105**:13–21.
12 Woo EY, Yeh H, Chu CS, Schlienger K, Carroll RG, Riley JL, Kaiser LR, June CH. Cutting edge: regulatory T cells from lung cancer patients directly inhibit autologous T cell proliferation. *J Immunol* 2002; **168**:4272–6.
13 Azuma H, Yamada Y, Shibuya-Fujiwara N *et al.* Functional evaluation of ex vivo expanded cord blood lymphocytes: possible use for adoptive cellular immunotherapy. *Exp Hematol* 2002; **30**:346–51.
14 Afzali B, Lombardi G, Lechler RI, Lord GM. The role of T helper 17 (Th17) and regulatory T cells (Treg) in human organ transplantation and autoimmune disease. *Clin Exp Immunol* 2007; **148**:32–46.
15 Castellino F, Germain RN. Cooperation between CD4+ and CD8+ T cells: when, where, and how. *Annu Rev Immunol* 2006; **24**:519–40.
16 Reiner SL. Development in motion: helper T cells at work. *Cell* 2007; **129**:33–6.
17 Bi Y, Liu G, Yang R. Th17 cell induction and immune regulatory effects. *J Cell Physiol* 2007; **211**:273–8.
18 Fossiez F, Djossou O, Chomarat P *et al.* T cell interleukin-17 induces stromal cells to produce proinflammatory and hematopoietic cytokines. *J Exp Med* 1996; **183**:2593–603.
19 Loong CC, Hsieh HG, Lui WY, Chen A, Lin CY. Evidence for the early involvement of interleukin 17 in human and experimental renal allograft rejection. *J Pathol* 2002; **197**:322–32.
20 Van Kooten C, Boonstra JG, Paape ME *et al.* Interleukin-17 activates human renal epithelial cells in vitro and is expressed during renal allograft rejection. *J Am Soc Nephrol* 1998; **9**:1526–34.
21 Vanaudenaerde BM, Dupont LJ, Wuyts WA *et al.* The role of interleukin-17 during acute rejection after lung transplantation. *Eur Respir J* 2006; **27**:779–87.
22 Ivanov II, McKenzie BS, Zhou L, Tadokoro CE, Lepelley A, Lafaille JJ, Cua DJ, Littman DR. The orphan nuclear receptor RORgammat directs the differentiation program of proinflammatory IL-17+ T helper cells. *Cell* 2006; **126**:1121–33.
23 Langrish CL, Chen Y, Blumenschein WM *et al.* IL-23 drives a pathogenic T cell population that induces autoimmune inflammation. *J Exp Med* 2005; **201**:233–40.
24 Oppmann B, Lesley R, Blom B *et al.* Novel p19 protein engages IL-12p40 to form a cytokine, IL-23, with biological activities similar as well as distinct from IL-12. *Immunity* 2000; **13**: 715–25.

25 Dieckmann D, Plottner H, Berchtold S, Berger T, Schuler G. Ex vivo isolation and characterization of CD4(+) CD25(+) T cells with regulatory properties from human blood. *J Exp Med* 2001; **193**:1303–10.

26 Wing K, Lindgren S, Kollberg G, Lundgren A, Harris RA, Rudin A, Lundin S, Suri-Payer E. CD4 T cell activation by myelin oligodendrocyte glycoprotein is suppressed by adult but not cord blood CD25+ T cells. *Eur J Immunol* 2003; **33**:579–87.

27 Wan YY, Flavell RA. Identifying Foxp3-expressing suppressor T cells with a bicistronic reporter. *Pro Natl Acad Sci USA* 2005; **102**:5126–31.

28 Read S, Greenwald R, Izcue A, Robinson N, Mandelbrot D, Francisco L, Sharpe AH, Powrie F. Blockade of CTLA-4 on CD4+ CD25+ regulatory T cells abrogates their function in vivo. *J Immunol* 2006; **177**:4376–83.

29 Hack CJ. Integrated transcriptome and proteome data: the challenges ahead. *Brief Funct Genomic Proteomic* 2004; **3**:212–9.

Gain-of-function of mutated *C-CBL* tumour suppressor in myeloid neoplasms

Masashi Sanada[1,5]*, Takahiro Suzuki[7]*, Lee-Yung Shih[8]*, Makoto Otsu[9], Motohiro Kato[1,2], Satoshi Yamazaki[6], Azusa Tamura[1], Hiroaki Honda[11], Mamiko Sakata-Yanagimoto[12], Keiki Kumano[3], Hideaki Oda[13], Tetsuya Yamagata[14], Junko Takita[1,2,3], Noriko Gotoh[10], Kumi Nakazaki[1,4], Norihiko Kawamata[15], Masafumi Onodera[16], Masaharu Nobuyoshi[7], Yasuhide Hayashi[17], Hiroshi Harada[18], Mineo Kurokawa[3,4], Shigeru Chiba[12], Hiraku Mori[18], Keiya Ozawa[7], Mitsuhiro Omine[18], Hisamaru Hirai[3,4], Hiromitsu Nakauchi[6,9], H. Phillip Koeffler[15] & Seishi Ogawa[1,5]

Acquired uniparental disomy (aUPD) is a common feature of cancer genomes, leading to loss of heterozygosity. aUPD is associated not only with loss-of-function mutations of tumour suppressor genes[1], but also with gain-of-function mutations of proto-oncogenes[2]. Here we show unique gain-of-function mutations of the *C-CBL* (also known as *CBL*) tumour suppressor that are tightly associated with aUPD of the 11q arm in myeloid neoplasms showing myeloproliferative features. The *C-CBL* proto-oncogene, a cellular homologue of *v-Cbl*, encodes an E3 ubiquitin ligase and negatively regulates signal transduction of tyrosine kinases[3–6]. Homozygous *C-CBL* mutations were found in most 11q-aUPD-positive myeloid malignancies. Although the *C-CBL* mutations were oncogenic in NIH3T3 cells, c-Cbl was shown to functionally and genetically act as a tumour suppressor. C-CBL mutants did not have E3 ubiquitin ligase activity, but inhibited that of wild-type C-CBL and CBL-B (also known as CBLB), leading to prolonged activation of tyrosine kinases after cytokine stimulation. *c-Cbl*$^{-/-}$ haematopoietic stem/progenitor cells (HSPCs) showed enhanced sensitivity to a variety of cytokines compared to *c-Cbl*$^{+/+}$ HSPCs, and transduction of *C-CBL* mutants into *c-Cbl*$^{-/-}$ HSPCs further augmented their sensitivities to a broader spectrum of cytokines, including stem-cell factor (SCF, also known as KITLG), thrombopoietin (TPO, also known as THPO), IL3 and FLT3 ligand (FLT3LG), indicating the presence of a gain-of-function that could not be attributed to a simple loss-of-function. The gain-of-function effects of C-CBL mutants on cytokine sensitivity of HSPCs largely disappeared in a *c-Cbl*$^{+/+}$ background or by co-transduction of wild-type *C-CBL*, which suggests the pathogenic importance of loss of wild-type *C-CBL* alleles found in most cases of *C-CBL*-mutated myeloid neoplasms. Our findings provide a new insight into a role of gain-of-function mutations of a tumour suppressor associated with aUPD in the pathogenesis of some myeloid cancer subsets.

Myelodysplastic syndromes (MDS) are heterogeneous groups of blood cancers originating from haematopoietic precursors. They are characterized by deregulated haematopoiesis showing a high propensity to acute myeloid leukaemia (AML)[7]. Some MDS cases have overlapping clinico-pathological features with myeloproliferative disorders, and are now classified into myelodysplasia/myeloproliferative neoplasms (MDS/MPN) by the World Health Organization (WHO) classification[8]. To obtain a comprehensive profile of allelic imbalances in these myeloid neoplasms, we performed allele-specific copy number analyses of bone marrow samples obtained from 222 patients with MDS, MDS/MPN, or other related myeloid neoplasms (Supplementary Tables 1 and 2) using high-density single nucleotide polymorphism (SNP) arrays combined with CNAG/AsCNAR software[9,10].

Genomic profiles of MDS and MDS/MPN showed characteristic unbalanced genetic changes, as reported in previous cytogenetic studies[11] (Supplementary Fig. 1a); however, they were detected more sensitively by SNP array analyses (Supplementary Table 3). aUPD was detected in 70 samples (31.5%) on the basis of the allele-specific copy number analyses, which substantially exceeded the detection rate obtained using a SNP call-based detection algorithm (20.7%) (Supplementary Figs 2 and 4, and Supplementary Tables 4 and 5). Long stretches of homozygous SNP calls caused by shared identical-by-descent alleles in parents were empirically predicted and excluded (Supplementary Fig. 3). aUPDs were more common in MDS/MPN than in MDS. They preferentially affected several chromosomal arms (1p, 1q, 4q, 7q, 11p, 11q, 14q, 17p and 21q) in distinct subsets of patients, and frequently associated with mutated oncogenes and tumour suppressor genes (Supplementary Figs 1b and 5). Among these, the most common aUPDs were those involving 11q ($n = 17$), which defined a unique subset of myeloid neoplasms that were clinically characterized by frequent diagnosis of chronic myelomonocytic leukaemia (CMML) with normal karyotypes (13 cases) (Fig. 1a and Supplementary Table 6). We identified a minimum overlapping aUPD segment of approximately 1.4 megabases (Mb) in 11q, which contained a mutated *C-CBL* proto-oncogene (Fig. 1b).

[1]Cancer Genomics Project, [2]Department of Pediatrics, [3]Cell Therapy and Transplantation Medicine, and [4]Hematology and Oncology, Graduate School of Medicine, The University of Tokyo, 7-3-1 Hongo, Bunkyo-ku, Tokyo 113-8655, Japan. [5]Core Research for Evolutional Science and Technology, [6]Exploratory Research for Advanced Technology, Japan Science and Technology Agency, 4-1-8 Honcho, Kawaguchi-shi, Saitama 332-0012, Japan. [7]Division of Hematology, Department of Medicine, Jichi Medical University, 3311-1 Yakushiji, Shimotsuke-shi, Tochigi 329-0498, Japan. [8]Division of Hematology-Oncology, Department of Internal Medicine, Chang Gung Memorial Hospital, Chang Gung University, 199 Tung Hwa North Road, Taipei 105, Taiwan. [9]Division of Stem Cell Therapy, Center for Stem Cell and Regenerative Medicine, [10]Division of Systems Biomedical Technology, Institute of Medical Science, The University of Tokyo, 4-6-1 Shirokanedai, Minato-ku, Tokyo 108-8639, Japan. [11]Department of Developmental Biology, Research Institute of Radiation Biology and Medicine, Hiroshima University, 1-2-3 Kasumi, Minami-ku, Hiroshima 734-8553, Japan. [12]Department of Clinical and Experimental Hematology, Institute of Clinical Medicine, University of Tsukuba, 1-1-1 Tennodai, Tukuba-shi, Ibaraki, 305-8571, Japan. [13]Department of Pathology, Tokyo Women's Medical University, 8-1 Kawada-cho, Shinjuku-ku, Tokyo 162-8666, Japan. [14]Department of Hematology, Dokkyo University School of Medicine, 800 Kitabayashi, Mibu, Tochigi 321-0293, Japan. [15]Hematology/Oncology, Cedars-Sinai Medical Center, 8700 Beverly Boulevard, Los Angeles, California 90048, USA. [16]Department of Genetics, National Research Institute for Child Health and Development, 2-10-1 Okura, Setagaya-ku, Tokyo, 157-8535, Japan. [17]Gunma Children's Medical Center, 779 Shimohakoda, Hokkitsu-machi, Shibukawa-shi, Gunma 377-8577, Japan. [18]Division of Hematology, Internal Medicine, Showa University Fujigaoka Hospital, 1-30 Fujigaoka, Aoba-ku, Yokohama, Kanagawa 227-8501, Japan.
*These authors contributed equally to this work.

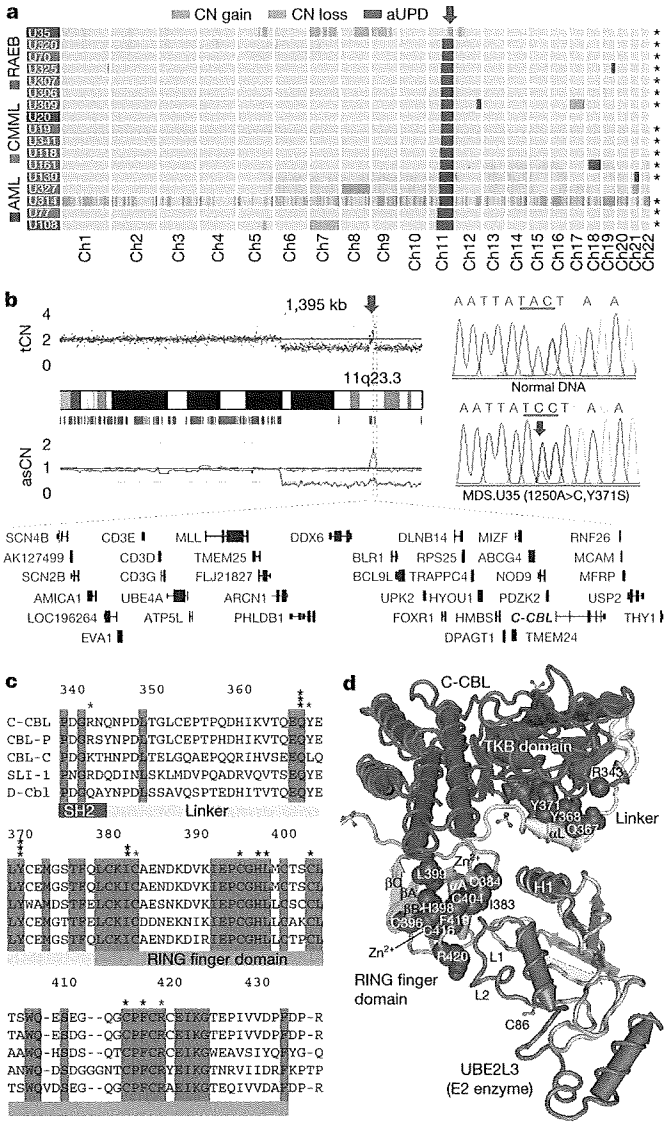

Figure 1 | Common UPD on the 11q arm and *C-CBL* mutations in myeloid neoplasms. **a**, Copy number profiles of 17 cases with myeloid neoplasms showing 11qUPD. Regions of copy number (CN) gains, losses and aUPD are depicted in different colours. Histologies are shown by coloured boxes. Asterisks denote *C-CBL*-mutated cases. Ch, chromosome; RAEB, refractory anaemia with excess blasts. **b**, CNAG output for MDS.U35. Total copy number (tCN) and allele-specific copy number (asCN) plots show a focal copy number gain spanning a 1.4-Mb segment within 3 Mb of an 11q-aUPD region (left), which contained mutated *C-CBL* in MDS.U35 (right). **c**, Alignments of amino acid sequences for human CBL family proteins and their homologues in *Caenorhabditis elegans* (SLI-1) and *Drosophila* (D-Cbl). Amino acid numbering is on the basis of human *C-CBL*. Conserved amino acids are highlighted. Positions of mutated amino acids are indicated by asterisks. Heterozygous mutations are shown in red. **d**, Mutated amino acid positions in the three-dimensional structure of a human C-CBL–UBE2L3 complex. TKB, tyrosine kinase binding domain.

C-CBL is the cellular homologue of the *v-Cbl* transforming gene of the Cas NS-1 murine leukaemia virus[5,12]. It was recently found to be mutated in human AML cases[13–15]. Together with its close homologue, CBL-B, C-CBL is thought to be involved in the negative modulation of tyrosine kinase signalling, primarily through their E3 ubiquitin ligase activity that is responsible for the downregulation of activated tyrosine kinases[3–5]. By sequencing all *C-CBL* exons in all 222 samples, we found *C-CBL* mutations in 15 of the 17 cases with 11q-aUPD, whereas only 3 out of 205 cases without 11q-aUPD had *C-CBL* mutations, showing a strong association of *C-CBL* mutations with 11q-aUPD ($P = 1.46 \times 10^{-18}$) (Supplementary Fig. 6 and Supplementary Tables 6 and 7), as also indicated in a recent report[16]. Thus, *C-CBL* was thought to be the major, if not the only, target of 11q-aUPD in myeloid neoplasms. Two different *C-CBL* mutations co-existed in three cases (Supplementary Fig. 6b). Somatic origins of the mutations were confirmed in three evaluable cases (Supplementary Fig. 6c).

In most cases, *C-CBL* mutations were missense, involving the evolutionarily conserved amino acids within the linker-RING finger domain that is central to the E3 ubiquitin ligase activity[17] (Fig. 1c). Another case with a predominant Cys384Tyr mutation also contained a nonsense mutation (Arg343X) in a minor subclone, which resulted in a v-Cbl-like truncated protein (Supplementary Fig. 6b). In the remaining two cases, mutations led to amino acid deletions (Δ369−371 and Δ368−382) involving the highly conserved α-helix (αL) of the linker domain and the first loop of the RING finger. According to the published crystal structure of *C-CBL*[17], most of the mutated or deleted amino acids were positioned on the interface for the binding to the E2 enzyme (Fig. 1d), making contact with either the tyrosine kinase binding domain (Tyr 368 and Tyr 371) or E2 ubiquitin-conjugating enzymes (Ile 383, Cys 404 and Phe 418). Especially, all seven linker-domain mutations selectively involved just three amino acids (Gln 367, Tyr 368 and Tyr 371) within the conserved αL helix (Fig. 1d). Mutations were clearly homozygous in nine cases, and the apparently heterozygous chromatograms in the other six cases could also be compatible with homozygous mutations affecting the aUPD-positive tumour clones, given the presence of substantial normal cell components within these samples. Mutations in the remaining three cases were considered to be heterozygous. About half of the *C-CBL*-mutated cases carried coexisting mutations of *RUNX1* (four cases), *TP53* (one case), *FLT3* internal tandem duplication (1 case) or *JAK2* (3 cases). *NRAS* and *KRAS* mutations were prevalent among CMML (15.1%) but occurred within discrete clusters from *C-CBL*-mutated cases (Supplementary Tables 2 and 6 and Supplementary Fig. 5). The mutation status of *C-CBL* did not substantially affect the clinical outcome (Supplementary Fig. 7).

All tested *C-CBL* mutants induced clear oncogenic phenotypes in NIH3T3 fibroblasts, as demonstrated by enhanced colony formation in soft agar and tumour generation in nude mice (Supplementary Fig. 8). Transformed NIH3T3 cells showed PI3 kinase-dependent activation of Akt and the transformed phenotype was reverted by treatment with the PI3 kinase inhibitor Ly294002 (Supplementary Fig. 9). When introduced into $Lin^- Sca1^+ c\text{-}Kit^+$ (LSK) HSPCs, C-CBL mutants (C-CBL(Gln367Pro) and C-CBL(Tyr371Ser)), as well as a mouse lymphoma-derived oncogenic mutant (C-CBL(70Z)), significantly promoted the replating capacity of these progenitors (Fig. 2a). Because c-Cbl negatively modulates tyrosine kinase signalling, and all *C-CBL* mutations, including those previously reported[13–16], affected the critical domains for its enzymatic activity involved in this modulation, C-CBL was postulated to have a tumour suppressor function; loss-of-function could be a mechanism for the oncogenicity of these C-CBL mutants[3,5]. To assess this possibility and to clarify further the role of *C-CBL* mutations in the pathogenesis of myeloid neoplasms, we generated *c-Cbl*$^{-/-}$ mice and examined their haematological phenotypes (Supplementary Fig. 10).

In agreement with previous reports[18–20], *c-Cbl*$^{-/-}$ mice exhibited splenomegaly and an augmented haematopoietic progenitor pool, as was evident from the increased colony formation of bone marrow cells in methylcellulose culture and higher numbers of LSK and CD34-negative LSK cells in bone marrow and/or spleen compared to their wild-type littermates (Fig. 2b–d and Supplementary Fig. 11). Furthermore, when introduced into a *BCR-ABL* transgenic background[21], the *c-Cbl*$^{-/-}$ allele accelerated blastic crisis depending on the allele dosage (Fig. 2e, f). These observations supported the notion that wild-type *C-CBL* has tumour suppressor functions, whereas 'mutant' *C-CBL* acts as an oncogene; *C-CBL* can therefore be both a proto-oncogene and a tumour suppressor gene.

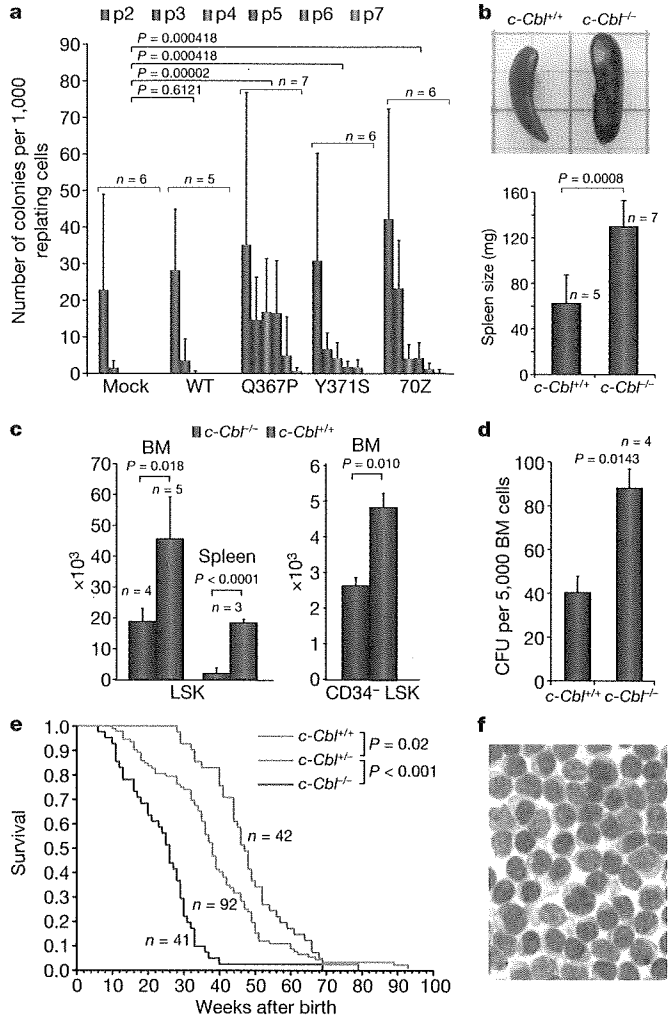

Figure 2 | Tumour-suppressor functions of wild-type C-CBL. **a**, Prolonged replating capacity of LSK cells transduced with mutant *C-CBL* (*C-CBL*(Gln367Pro) and *C-CBL*(Tyr371Ser)), compared to mock- or wild-type *C-CBL*-transduced cells. Replating capacity in methylcellulose culture is shown as mean colony number (and s.d.) per 1,000 replating cells at indicated times of replating. p, passage. **b**, Increased spleen mass in *c-Cbl*$^{-/-}$ mice compared to *c-Cbl*$^{+/+}$ mice (mean spleen weight and s.d.). **c**, Mean number of total LSK (left) and CD34-negative LSK (right) cells (plus s.d.) in bone marrow (BM) and/or spleen in *c-Cbl*$^{+/+}$ (blue columns) and *c-Cbl*$^{-/-}$ mice (red columns). Bone marrow cells from bilateral tibias and femurs were counted for each mouse. **d**, Augmented colony-forming potential of bone marrow cells from *c-Cbl*$^{-/-}$ mice (mean colony number and s.d. per 5,000 bone marrow cells). CFU, colony-forming units. **e**, Kaplan–Meier survival curves of *c-Cbl*$^{+/+}$, *c-Cbl*$^{+/-}$ and *c-Cbl*$^{-/-}$ mice carrying a *BCR-ABL* transgene, showing acceleration of blastic crisis in *c-Cbl*$^{+/-}$ and *c-Cbl*$^{-/-}$ mice. **f**, Wright–Giemsa staining of an enlarged lymph node in a *Bcr-Abl*$^{+}$ *c-Cbl*$^{-/-}$ mouse during blastic crisis shows massive infiltrates of immature leukaemic blasts. Original magnification, ×600.

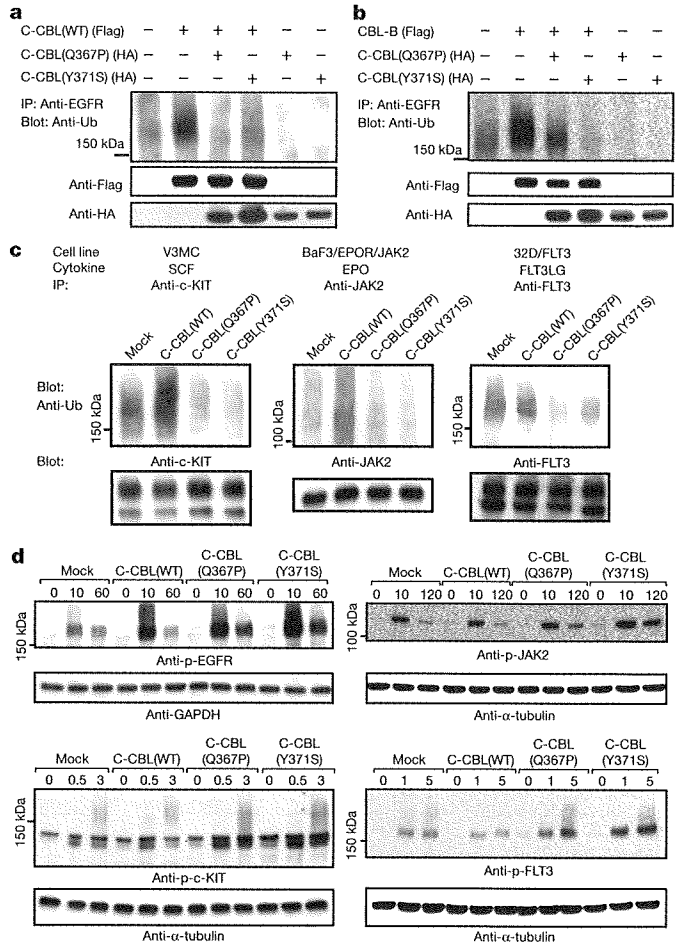

Figure 3 | Inhibitory actions of C-CBL mutants on wild-type C-CBL. **a**, **b**, Flag-tagged wild-type C-CBL (**a**) or CBL-B (**b**) were transfected into NIH3T3 cells stably transduced with human EGFR plus indicated HA-tagged C-CBL mutants. Anti-ubiquitin blots of immunoprecipitated EGFR after EGF stimulation show the inhibitory actions of the C-CBL mutants on ubiquitinating activity of C-CBL (**a**) and CBL-B (**b**). Bottom panels are anti-HA and anti-Flag blots of total cell lysates. **c**, Effects of wild-type and mutant C-CBL on cytokine-induced ubiquitination of c-KIT, JAK2 and FLT3 in haematopoietic cells V3MC, BaF3 co-transduced with human erythropoietin receptor (EPOR) and JAK2 (BaF3/EPOR/JAK2), and FLT3-transduced 32D (32D/FLT3), respectively. Each cell line was further transduced with indicated C-CBL mutants, and ubiquitination of immunoprecipitated kinases was detected by anti-ubiquitin blots at 1 min after stimulation with SCF, EPO and FLT3LG. Anti-kinase blots of the precipitated kinases are shown below each panel. **d**, Kinase phosphorylation was examined at indicated time points (shown in minutes) after ligand stimulation using immunoblot analyses of total cell lysates using antibodies to phosphorylated (p-) EGFR, c-KIT, JAK2 and FLT3 in which anti-α-tubulin or anti-GAPDH blots are provided as a control.

Mouse LSK HSPCs expressed two Cbl family member proteins: wild-type c-Cbl and Cbl-b (Supplementary Fig. 12)[22]. When transduced into NIH3T3 cells stably expressing human epidermal growth factor receptor (EGFR), both Cbl proteins enhanced ubiquitination of EGFR after EGF stimulation, which was suppressed by coexpression of the C-CBL mutants (Fig. 3a, b). In haematopoietic cells, overexpression of wild-type C-CBL enhanced ligand-induced ubiquitination of a variety of tyrosine kinases, including c-KIT, FLT3 and JAK2. In contrast, C-CBL mutants not only showed compromised enzymatic activity, but also inhibited the ubiquitinating activities in these haematopoietic cells (Fig. 3c), leading to prolonged tyrosine kinase activation after ligand stimulation (Fig. 3d).

Because tyrosine kinase signalling is central to cytokine responses in haematopoietic cells and its deregulation is a common feature of myeloproliferative disorders[23], we next examined the effects of *C-CBL* mutations (*C-CBL*(Gln367Pro) and *C-CBL*(Tyr371Ser)) and the loss of wild-type *C-CBL* alleles on the responses of LSK HSPCs to various cytokines. In serum-free conditions, *c-Cbl*$^{-/-}$ LSK cells showed a modestly enhanced proliferative response to a variety of cytokines, including SCF, IL3 and TPO, compared to *c-Cbl*$^{+/+}$ cells (mock columns in Fig. 4a). However, the enhanced response in *c-Cbl*$^{-/-}$ cells was markedly augmented and extended to a broader spectrum of cytokines, including FLT3 ligand by the transduction of *C-CBL* mutants. Of note, the effect of *C-CBL* mutant transduction was not remarkable in *c-Cbl*$^{+/+}$ LSK cells except for the response to SCF, which was clearly enhanced by *C-CBL* mutants

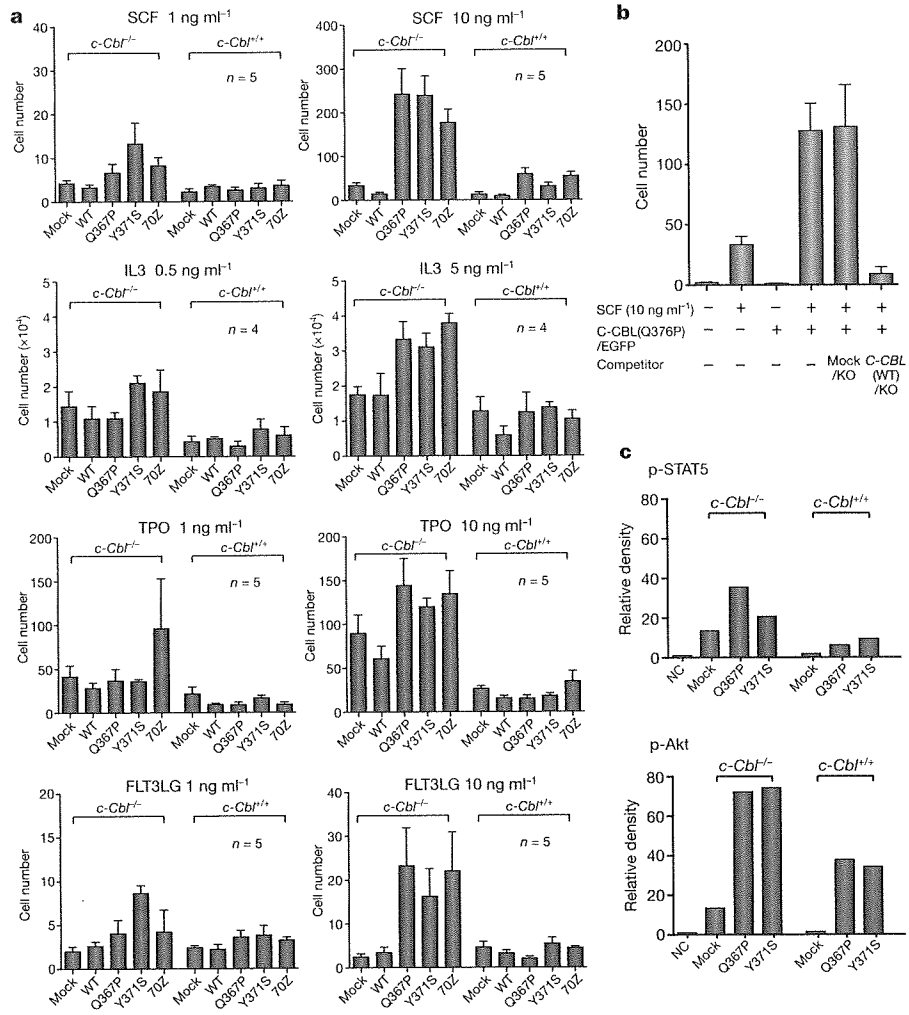

Figure 4 | Gain-of-function of mutant C-CBL augmented by loss of wild-type C-CBL. **a**, *c-Cbl*$^{+/+}$ and *c-Cbl*$^{-/-}$ LSK cells were transfected with various *C-CBL* internal ribosome entry site (IRES)/green fluorescent protein (GFP) constructs, and 50 GFP-positive cells were sorted for serum-free culture containing indicated concentrations of SCF, IL3, TPO and FLT3LG. Mean cell numbers (plus s.e.m.) on day 5 are plotted. **b**, *c-Cbl*$^{-/-}$ LSK cells were co-transduced with C-CBL(Gln367Pro)-IRES-EGFP (C-CBL(Q367P)/EGFP) and mock-IRES-Kusabira-Orange (mock/KO) or wild-type *C-CBL*-IRES-Kusabira-Orange (*C-CBL*(WT)/KO), and 50 GFP/KO double-positive cells were sorted into each well for cell proliferation assays in serum-free culture containing 10 ng ml^{-1} SCF. Mean cell numbers on day 5 (plus s.e.m., $n = 5$) are plotted. **c**, Ten thousand *c-Cbl*$^{+/+}$ and *c-Cbl*$^{-/-}$ LSK cells transduced with various C-CBL constructs were stimulated with 10 ng ml^{-1} SCF and 10 ng ml^{-1} TPO for 15 min. Total cell lysates were analysed by immunoblotting, using antibodies to STAT5, Akt and their phosphorylated forms. The intensities of phosphorylated proteins relative to total STAT5 (top panel) and Akt (bottom panel) are plotted. NC indicates the mean background signal obtained with nonspecific IgG.

even with a *c-Cbl*$^{+/+}$ background (Fig. 4a and Supplementary Fig. 13). To clarify further the effect of wild-type C-CBL on C-CBL mutants, both wild-type C-CBL and C-CBL mutants were co-transduced into *c-Cbl*$^{-/-}$ LSK cells, and their effects on the response to SCF were examined. As shown in Fig. 4b, the hyperproliferative response induced by C-CBL mutants was almost completely abolished by the co-transduction of wild-type C-CBL, suggesting the pathogenic importance of loss of wild-type *C-CBL* alleles found in most *C-CBL*-mutated cases. LSK cells transduced with C-CBL mutants also showed enhanced activation of the STAT5 and Akt pathways on cytokine stimulation (SCF and TPO), which was more pronounced in *c-Cbl*$^{-/-}$ than *c-Cbl*$^{+/+}$ LSK cells (Fig. 4c and Supplementary Fig. 14).

The modest enhancement of sensitivity to cytokines found in *c-Cbl*$^{-/-}$ LSK cells was a consequence of loss of C-CBL functions. In contrast, the hypersensitive response of mutant-transduced *c-Cbl*$^{-/-}$ LSK cells to a broad spectrum of cytokines represents gain-of-function of the mutants that could not be ascribed to a simple loss of C-CBL functions, which was also predicted from the strong association of *C-CBL* mutations with 11q-aUPD by analogy to the gain-of-function *JAK2* mutations associated with 9p-aUPD in polycythemia vera[2]. The gain-of-function of C-CBL mutants became more evident under a *c-Cbl*$^{-/-}$ background. The hypersensitive response to cytokines induced by mutant C-CBL under the *c-Cbl*$^{-/-}$ background was largely offset by the presence of the wild-type *c-Cbl* allele or by the transduction of the wild-type C-CBL gene, suggesting that the gain-of-function could be closely related to loss of C-CBL-like functions, probably by inhibition of Cbl-b. Supporting this view is a previous report that *c-Cbl/Cbl-b* double knockout T cells showed more profound impairments in the downregulation of the T-cell receptor (TCR), more sustained TCR signalling, and more vigorous proliferation, than *c-Cbl* or *Cbl-b* single knockout T cells after anti-CD3 (also known as CD3e) stimulation[24]. This is analogous to the gain-of-function found in some TP53 mutants, which has been explained by functional inhibition of two TP53 homologues, TP73 and TP63 (refs 25, 26). Of note, TP53 was also originally isolated as an oncogene through its mutated forms[27]. The Cbl-b inhibition-based gain-of-function model could be tested directly by comparing the behaviour of *c-Cbl/Cbl-b* double knockout LSK cells with that of LSK cells carrying homozygously knocked-in mutant *C-CBL* alleles. On the other hand, there remains a possibility that the gain-of-function could be mediated by a mechanism other than the simple inhibition of the homologue, because C-CBL mutants retained several motifs

that interacted with numerous signal-transducing molecules. Furthermore, considering the ubiquitous expression of CBL proteins, it would be of interest to explore the possible involvement of mutations in all *CBL* family members in other human cancers.

METHODS SUMMARY

Genomic DNA from 222 bone marrow samples with myeloid neoplasms were analysed using GeneChip SNP-genotyping microarrays (Affymetrix GeneChip) as described[28]. Allelic imbalances were detected from the allele-specific copy numbers calculated using CNAG/AsCNAR software (http://www.genome.umin.jp)[9,10]. *C-CBL* mutations were examined by sequencing PCR-amplified genomic DNA. For functional assays, haemagglutinin (HA)- or Flag-tagged complementary DNAs of wild-type and mutant *C-CBL* were generated by *in vitro* mutagenesis, constructed into a MSCV-based retroviral vector, pGCDNsamIRESGFP or pGCDNsamIRESKO, and used for retrovirus-mediated gene transfer. For the evaluation of oncogenicity of C-CBL mutants, NIH3T3 cells were transfected with various *C-CBL* constructs and used for colony assays in soft agar and tumour formation assays in nude mice. *c-Cbl*-deficient mice were generated using a conventional strategy of gene-targeting and crossed with *BCR-ABL* transgenic mice to evaluate the effect of the $c\text{-}Cbl^{-}$ allele on the acceleration of blastic crisis. LSK cells sorted from $c\text{-}Cbl^{+/+}$ and $c\text{-}Cbl^{-/-}$ mice were transduced with various *C-CBL* constructs. Their responses to cytokines were evaluated by cell proliferation assays, followed by immunoblot analyses of c-KIT, FLT3 and JAK2, as well as their downstream signalling molecules. The effects of C-CBL mutant expression on the ubiquitination of EGFR, c-KIT, FLT3 and JAK2 were examined by transducing C-CBL mutants into relevant cells, followed by anti-ubiquitin blots of the immunoprecipitated kinases after ligand stimulation. Functional competition of C-CBL mutants with wild-type C-CBL was assessed by cell proliferation assays of LSK cells co-transduced with both wild-type and mutant C-CBL genes. This study was approved by the ethics boards of the University of Tokyo, Chang Gung Memorial Hospital and Showa University. Antibodies and primers used in this study are listed in Supplementary Tables 8 and 9.

Full Methods and any associated references are available in the online version of the paper at www.nature.com/nature.

Received 9 October 2008; accepted 30 June 2009.
Published online 20 July 2009.

1. Knudson, A. G. Two genetic hits (more or less) to cancer. *Nature Rev. Cancer* **1**, 157–162 (2001).
2. James, C. *et al.* A unique clonal JAK2 mutation leading to constitutive signalling causes polycythaemia vera. *Nature* **434**, 1144–1148 (2005).
3. Ryan, P. E. *et al.* Regulating the regulator: negative regulation of Cbl ubiquitin ligases. *Trends Biochem. Sci.* **31**, 79–88 (2006).
4. Schmidt, M. H. & Dikic, I. The Cbl interactome and its functions. *Nature Rev. Mol. Cell Biol.* **6**, 907–918 (2005).
5. Thien, C. B. & Langdon, W. Y. Cbl: many adaptations to regulate protein tyrosine kinases. *Nature Rev. Mol. Cell Biol.* **2**, 294–307 (2001).
6. Thien, C. B. & Langdon, W. Y. c-Cbl and Cbl-b ubiquitin ligases: substrate diversity and the negative regulation of signalling responses. *Biochem. J.* **391**, 153–166 (2005).
7. Corey, S. J. *et al.* Myelodysplastic syndromes: the complexity of stem-cell diseases. *Nature Rev. Cancer* **7**, 118–129 (2007).
8. Jaffe, E., Harris, N., Stein, H. & Vardiman J. *World Health Organization Classification of Tumours: Pathology and Genetics of Tumours of Haematopoietic and Lymphoid Tissues* 62–73 (IARC Press, 2002).
9. Nannya, Y. *et al.* A robust algorithm for copy number detection using high-density oligonucleotide single nucleotide polymorphism genotyping arrays. *Cancer Res.* **65**, 6071–6079 (2005).
10. Yamamoto, G. *et al.* Highly sensitive method for genomewide detection of allelic composition in nonpaired, primary tumor specimens by use of affymetrix single-nucleotide-polymorphism genotyping microarrays. *Am. J. Hum. Genet.* **81**, 114–126 (2007).
11. Haase, D. Cytogenetic features in myelodysplastic syndromes. *Ann. Hematol.* **87**, 515–526 (2008).
12. Langdon, W. Y. *et al.* v-cbl, an oncogene from a dual-recombinant murine retrovirus that induces early B-lineage lymphomas. *Proc. Natl Acad. Sci. USA* **86**, 1168–1172 (1989).
13. Abbas, S. *et al.* Exon 8 splice site mutations in the gene encoding the E3-ligase CBL are associated with core binding factor acute myeloid leukemias. *Haematologica* **93**, 1595–1597 (2008).
14. Caligiuri, M. A. *et al.* Novel c-CBL and CBL-b ubiquitin ligase mutations in human acute myeloid leukemia. *Blood* **110**, 1022–1024 (2007).
15. Sargin, B. *et al.* Flt3-dependent transformation by inactivating c-Cbl mutations in AML. *Blood* **110**, 1004–1012 (2007).
16. Dunbar, A. J. *et al.* 250K single nucleotide polymorphism array karyotyping identifies acquired uniparental disomy and homozygous mutations, including novel missense substitutions of c-Cbl, in myeloid malignancies. *Cancer Res.* **68**, 10349–10357 (2008).
17. Zheng, N. *et al.* Structure of a c-Cbl-UbcH7 complex: RING domain function in ubiquitin-protein ligases. *Cell* **102**, 533–539 (2000).
18. Murphy, M. A. *et al.* Tissue hyperplasia and enhanced T-cell signalling via ZAP-70 in c-Cbl-deficient mice. *Mol. Cell. Biol.* **18**, 4872–4882 (1998).
19. Naramura, M. *et al.* Altered thymic positive selection and intracellular signals in Cbl-deficient mice. *Proc. Natl Acad. Sci. USA* **95**, 15547–15552 (1998).
20. Rathinam, C. *et al.* The E3 ubiquitin ligase c-Cbl restricts development and functions of hematopoietic stem cells. *Genes Dev.* **22**, 992–997 (2008).
21. Honda, H. *et al.* Acquired loss of p53 induces blastic transformation in p210(bcr/abl)-expressing hematopoietic cells: a transgenic study for blast crisis of human CML. *Blood* **95**, 1144–1150 (2000).
22. Zeng, S. *et al.* Regulation of stem cell factor receptor signaling by Cbl family proteins (Cbl-b/c-Cbl). *Blood* **105**, 226–232 (2005).
23. Kaushansky, K. Hematopoietic growth factors, signaling and the chronic myeloproliferative disorders. *Cytokine Growth Factor Rev.* **17**, 423–430 (2006).
24. Naramura, M. *et al.* c-Cbl and Cbl-b regulate T cell responsiveness by promoting ligand-induced TCR down-modulation. *Nature Immunol.* **3**, 1192–1199 (2002).
25. Dittmer, D. *et al.* Gain of function mutations in p53. *Nature Genet.* **4**, 42–46 (1993).
26. Lang, G. A. *et al.* Gain of function of a p53 hot spot mutation in a mouse model of Li-Fraumeni syndrome. *Cell* **119**, 861–872 (2004).
27. Finlay, C. A., Hinds, P. W. & Levine, A. J. The p53 proto-oncogene can act as a suppressor of transformation. *Cell* **57**, 1083–1093 (1989).
28. Chen, Y. *et al.* Oncogenic mutations of ALK kinase in neuroblastoma. *Nature* **455**, 971–974 (2008).

Supplementary Information is linked to the online version of the paper at www.nature.com/nature.

Acknowledgements This work was supported by the Core Research for Evolutional Science and Technology, Japan Science and Technology Agency, a Grant-in-Aid from the Ministry of Health, Labor and Welfare of Japan and from the Ministry of Education, Culture, Sports, Science and Technology, and a grant from National Health Research Institute, Taiwan, NHRI-EX96-9434SI, and NIH-2R01CA026038-30. We thank W. Y. Langdon for providing a human *C-CBL* cDNA. A mast-cell cell line expressing c-KIT V3MC was a gift from M. F. Gurish. We also thank Y. Ogino and K. Fujita for their technical assistance.

Author Contributions M.S. and M.Kato performed microarray experiments and subsequent data analyses. T.S., T.Y., H.Honda and H.Hirai generated and analysed *c-Cbl*-null mice. M.S., M.Otsu, S.Y., M.N., K.K., N.G., M.Onodera, M.S.-Y. and H.N. conducted functional assays of C-CBL mutants. L.-Y.S., M.S., M.Kato, K.N., J.T. and A.T. performed mutation analysis. H.O. performed pathological analysis of *c-Cbl*-null mice. L.-Y.S., N.K., H.Harada, M.Kurokawa, S.C., H.M., H.P.K. and M.Omine prepared MDS specimens. M.S., M.Otsu, Y.H., K.O., H.M., H.N., L.-Y.S., H.P.K. and S.O. designed the overall study, and S.O. wrote the manuscript. All authors discussed the results and commented on the manuscript.

Author Information Full copy number data for the 222 samples are accessible from the Gene Expression Omnibus public database (http://ncbi.nlm.nih.gov/geo/) with the accession number GSE15187. Reprints and permissions information is available at www.nature.com/reprints. Correspondence and requests for materials should be addressed to S.O. (sogawa-tky@umin.ac.jp) or L.-Y.S. (sly7012@adm.cgmh.org.tw).

METHODS

Genome-wide analysis of allelic imbalances in primary myeloid neoplasms. Bone marrow specimens were obtained from 222 patients diagnosed with myeloid neoplasms according to the WHO classification (Supplementary Tables 1 and 2). High molecular weight genomic DNA was extracted and used for microarray analysis using Affymetrix GeneChip 50K XbaI, HindIII or 250K NspI, according to the manufacturer's instructions. Genome-wide detection of allelic imbalances was performed using CNAG/AsCNAR software (http://www.genome.umin.jp)[9,10].

Mutation analysis. Mutation analysis was performed by direct sequencing of PCR-amplified coding exons of the relevant genes, using an ABI PRISM 3100 genetic analyser (Applied Biosystems). The target genes, exons and PCR primers are listed in Supplementary Table 8. Tandem duplication of the *FLT3* gene was examined by genomic PCR and sequencing.

Preparation of high-titre vesicular stomatitis virus glycoprotein (VSV-G)-pseudotyped retroviral particles. HA-tagged human *C-CBL* cDNA was a gift from W. Y. Langdon. Nine mutant cDNAs of *C-CBL*, including eight from patients' specimens and a 70Z mutant corresponding to a mutant isolated from mouse lymphoma[29], were generated on the basis of this construct, using a QuickChange site-directed mutagenesis kit (Stratagene). These were then constructed into the retrovirus vectors pGCDNsamIRESGFP and pGCDNsamIRESKO[30–32]. Vector plasmids were co-transfected with a VSV-G cDNA into 293GP cells (provided by R. C. Mulligan) to obtain retrovirus-containing supernatant, which was then transduced into 293GPG cells to establish stable cell lines capable of producing VSV-G-pseudotyped retroviral particles on induction[33,34]. The average titre of retrovirus stocks prepared from these cell lines routinely exceeded approximately $1–10 \times 10^7$ inclusion-forming units per ml, as estimated using Jurkat cells.

Assays for anchorage-independent growth and tumorigenicity in nude mice. NIH3T3 cells (the Japan Cell Resource Bank) were stably transduced with wild-type and mutant *C-CBL* by retrovirus-mediated gene transfer. For colony formation assays, 1.0×10^3 stable cells for each construct were inoculated in 0.33% top agar, and the numbers of colonies >1 mm in diameter were counted 3 weeks after inoculation ($n = 8$). Experiments were repeated four times. For tumour formation in nude mice, 1.0×10^7 stable cells were inoculated subcutaneously at two sites per mouse. Cells were inoculated at six sites in three mice for each construct.

Purification of LSK HSPCs. LSK HSPCs were purified from bone marrow and spleen as described[35,36]. Multicolour flow cytometry analysis and cell sorting were performed using a MoFlo cell Sorter (Beckman Coulter). The purity of sorted cell fractions consistently exceeded 98%.

Replating assays of bone marrow progenitor cells. Bone marrow LSK cells were infected with IRES/GFP-containing retrovirus carrying mock, wild-type C-CBL and three C-CBL mutants (C-CBL(Gln367Pro), C-CBL(Tyr371Ser) and C-CBL(Cys384Gly)) as well as C-CBL(70Z) on RetroNectin-coated dishes. After 48 h infection in culture in StemSpan supplemented with SCF (50 ng ml^{-1}; Peprotech), TPO (20 ng ml^{-1}) and FLT3LG (20 ng ml^{-1}), 1.0×10^2 GFP-positive cells were inoculated in MethoCult M3231 supplemented with TPO (20 ng ml^{-1}), IL3 (10 ng ml^{-1}), IL6 (10 ng ml^{-1}), FLT3LG (10 ng ml^{-1}) and SCF (50 ng ml^{-1}) for colony formation. Colony-forming cells were collected 7 days after each inoculation, from which 1.0×10^3 cells were repeatedly subjected to replating until no colonies were produced. Experiments were repeated at the indicated times for each C-CBL construct.

Generation of *c-Cbl*$^{-/-}$ mice and evaluation of their tumour-prone phenotype. *c-Cbl*$^{-/-}$ mice were generated using a conventional method of gene targeting (Supplementary Fig. 10). *c-Cbl*$^{+/+}$, *c-Cbl*$^{+/-}$ and *c-Cbl*$^{-/-}$ mice were crossed with *BCR-ABL* transgenic mice, and their survival and the development of blastic crises were monitored.

Evaluation of haematopoietic pool size in *c-Cbl*$^{-/-}$ mice. LSK and CD34$^-$ LSK cells were sorted from bone marrow cells or spleens of *c-Cbl*$^{-/-}$ mice, and their numbers were compared to those in *c-Cbl*$^{+/+}$ littermates (8 week old). Approximately 5×10^3 bone marrow cells collected from *c-Cbl*$^{+/+}$ and *c-Cbl*$^{-/-}$ mice were inoculated into MethoCult M3231 culture supplemented with TPO (20 ng ml^{-1}), IL3 (10 ng ml^{-1}), IL6 (10 ng ml^{-1}), EPO (3 U ml^{-1}) and SCF (50 ng ml^{-1}). The number of colonies was counted 7 days after culturing.

***In vitro* cell proliferation assays.** Approximately 6×10^3 LSK cells from *c-Cbl*$^{-/-}$ mice and their *c-Cbl*$^{+/+}$ littermates (8 week old) were sorted into RetroNectin-coated 96-well U-bottom plates containing α-minimum essential medium supplemented with 1% fetal bovine serum (FBS), mouse SCF (50 ng ml^{-1}), and human TPO (100 ng ml^{-1}). After 24 h pre-incubation, retrovirus supernatant was added to each well at a multiplicity of infection of about 10. The plates were incubated for another 24 h in the presence of protamine sulphate (10 μg ml^{-1}), followed by repeated infection and extended culture for 2 days in S-Clone SF-O3 medium (Sanko Junyaku) supplemented with 1% BSA, 50 ng ml^{-1} SCF and 50 ng ml^{-1} TPO. On day 4, fluorescent-marker-positive cells were sorted for subsequent analyses. Cell survival and proliferation of LSK cells transduced with different *C-CBL* constructs were assessed in serum-free liquid culture in 96-well U-bottom plates in the presence of various cytokines. Each well received 50 fluorescent-marker-positive LSK cells, and the cells were cultured in S-Clone supplemented with 1% BSA plus SCF, TPO, IL3 or FLT3LG at the indicated concentrations. Cell numbers were counted either by analysing well images or by flow cytometry using FlowCount beads (Beckman Coulter). After 6 h serum starvation, 1×10^4 LSK cells transduced with various *C-CBL* constructs were stimulated with SCF (10 ng ml^{-1}) and TPO (10 ng ml^{-1}) for 15 min. Whole-cell lysates were examined for activation of STAT5 and Akt by immunoblots using the respective antibodies.

Immunoblot analysis of physical interactions between mutant C-CBL and CBL-B. Flag-tagged CBL-B or C-CBL was co-transfected into NIH3T3 cells with each of three HA-tagged C-CBL mutants (C-CBL(Gln367Pro), C-CBL(Tyr371Ser) and C-CBL(70Z)). Total cell lysates of these NIH3T3 cells were immunoprecipitated with anti-Flag antibody, followed by immunoblot analysis with anti-HA antibody.

Detection of ubiquitination and phosphorylation of kinases. After overnight serum starvation, NIH3T3 cells stably transduced with human EGFR, and indicated HA-tagged C-CBL mutants and Flag-tagged wild-type C-CBL were stimulated with human EGF (10 ng ml^{-1}) for 2 min. Cell lysates were immunoprecipitated with anti-EGF antibody, followed by immunoblotting using anti-ubiquitin antibody. Constructs for wild-type C-CBL and mutant C-CBL were stably transduced into a mast cell line, V3MC, FLT3-transduced 32D cells (32D/FLT3) and BaF3 cells transduced with human EPOR and JAK2 (BaF3/EPOR/JAK2) using retrovirus-mediated gene transfer. After overnight serum starvation, the transduced cells were stimulated with 10 ng ml^{-1} SCF (V3MC), 10 U ml^{-1} EPO (BaF3/EPOR/JAK2) or 10 ng ml^{-1} FLT3LG (32D/FLT3) for 1 min. The specific kinases were immunoprecipitated with relevant antibodies, and their ubiquitination was detected by immunoblotting with anti-ubiquitin antibody. Tyrosine phosphorylation of EGFR, c-KIT, JAK2 and FLT3 was examined by immunoblot analyses of total cell lysates after cytokine stimulation at indicated time points, using antibodies specifically recognizing phosphorylated kinases, anti-p-EGFR, anti-p-c-KIT, anti-p-JAK2 and anti-p-FLT3, respectively. Anti-GAPDH or anti-α-tubulin immunoblot was performed as a control. Antibodies used in this study are listed in Supplementary Table 9.

Statistical analysis. Statistical significance of prolonged replating capacity of mutant *C-CBL*-transduced LSK cells was tested by counting the total number of dishes that produced colonies, followed by Fisher's exact test. Survival curves of *c-Cbl*$^{+/+}$, *c-Cbl*$^{+/-}$ and *c-Cbl*$^{-/-}$ mice containing the *BCR-ABL* transgene were generated using the Kaplan–Meier method. Overall survivals of *C-CBL*-mutated and non-mutated CMML cases were analysed according to the proportional hazard model, using STATA software. Statistical differences in survival were evaluated using the log-rank test, and statistical differences in 2×2 contingency tables were tested according to Fisher's exact method. Student's *t*-tests were used to evaluate the significance of difference in spleen mass, number of haematopoietic progenitors and colony-forming cells between *c-Cbl*$^{+/+}$ and *c-Cbl*$^{-/-}$.

29. Blake, T. J. *et al.* The sequences of the human and mouse c-cbl proto-oncogenes show v-cbl was generated by a large truncation encompassing a proline-rich domain and a leucine zipper-like motif. *Oncogene* 6, 653–657 (1991).
30. Hamanaka, S. *et al.* Stable transgene expression in mice generated from retrovirally transduced embryonic stem cells. *Mol. Ther.* 15, 560–565 (2007).
31. Nabekura, T. *et al.* Potent vaccine therapy with dendritic cells genetically modified by the gene-silencing-resistant retroviral vector GCDNsap. *Mol. Ther.* 13, 301–309 (2006).
32. Sanuki, S. *et al.* A new red fluorescent protein that allows efficient marking of murine hematopoietic stem cells. *J. Gene Med.* 10, 965–971 (2008).
33. Ory, D. S., Neugeboren, B. A. & Mulligan, R. C. A stable human-derived packaging cell line for production of high titer retrovirus/vesicular stomatitis virus G pseudotypes. *Proc. Natl Acad. Sci. USA* 93, 11400–11406 (1996).
34. Suzuki, A. *et al.* Feasibility of *ex vivo* gene therapy for neurological disorders using the new retroviral vector GCDNsap packaged in the vesicular stomatitis virus G protein. *J. Neurochem.* 82, 953–960 (2002).
35. Ema, H. *et al.* Adult mouse hematopoietic stem cells: purification and single-cell assays *Nature Protoc.* 1, 2979–2987 (2006).
36. Osawa, M. *et al.* Long-term lymphohematopoietic reconstitution by a single CD34-low/negative hematopoietic stem cell. *Science* 273, 242–245 (1996).

Derivation of functional mature neutrophils from human embryonic stem cells

Yasuhisa Yokoyama,[1-3] Takahiro Suzuki,[1,2,4] Mamiko Sakata-Yanagimoto,[1-3] Keiki Kumano,[1,2] Katsumi Higashi,[5] Tsuyoshi Takato,[4] Mineo Kurokawa,[2] Seishi Ogawa,[1,4,6] and Shigeru Chiba[1,3]

[1]Department of Cell Therapy and Transplantation Medicine, University of Tokyo Hospital, Tokyo; [2]Department of Hematology and Oncology, Graduate School of Medicine, University of Tokyo, Tokyo; [3]Department of Clinical and Experimental Hematology, University of Tsukuba, Ibaraki; [4]Divison of Tissue Engineering, University of Tokyo Hospital, Tokyo; [5]Department of Clinical Hematology, School of Health Sciences, Kyorin University, Tokyo; and [6]The 21st Century COE Program, Graduate School of Medicine, University of Tokyo, Tokyo, Japan

Human embryonic stem cells (hESCs) proliferate infinitely and are pluripotent. Only a few reports, however, describe specific and efficient methods to induce hESCs to differentiate into mature blood cells. It is important to determine whether and how these cells, once generated, behave similarly with their in vivo–produced counterparts. We developed a method to induce hESCs to differentiate into mature neutrophils. Embryoid bodies were formed with bone morphogenic protein-4, stem cell factor (SCF), Flt-3 ligand (FL), interleukin-6 (IL-6)/IL-6 receptor fusion protein (FP6), and thrombopoietin (TPO). Cells derived from the embryoid bodies were cultured on a layer of irradiated OP9 cells with a combination of SCF, FL, FP6, IL-3, and TPO, which was later changed to granulocyte–colony-stimulating factor. Morphologically mature neutrophils were obtained in approximately 2 weeks with a purity and efficiency sufficient for functional analyses. The population of predominantly mature neutrophils (hESC-Neu's) showed superoxide production, phagocytosis, bactericidal activity, and chemotaxis similar to peripheral blood neutrophils from healthy subjects, although there were differences in the surface antigen expression patterns, such as decreased CD16 expression and aberrant CD64 and CD14 expression in hESC-Neu's. Thus, this is the first description of a detailed functional analysis of mature hESC-derived neutrophils. (Blood. 2009;113:6584-6592)

Introduction

Embryonic stem (ES) cells can self-renew and differentiate into cells derived from all 3 germ layers (ie, ectoderm, endoderm, and mesoderm). Both mouse and human ES cells give rise to mature blood cells of granulocyte/macrophage, erythroid, and megakaryoid lineages in vitro. For blood cell induction from ES cells, the majority of investigators use a coculturing system with mouse stromal cells such as S17[1] or OP9.[2,3] Embryoid body (EB) formation is also a commonly used method to obtain starting materials for further culture.[4-6] Cell surface antigens, such as CD45 and CD34, and colony-forming ability are used as blood cell markers. Hemangioblasts, which have the capacity to differentiate into both endothelial and blood cells, have also been produced.[7-9] Only a few studies, however, have achieved specific and effective induction of mature blood cells from ES cells, particularly human ES cells (hESCs).[10]

Human ESC-derived blood cells are potentially useful as a replacement for donation-based blood for transfusion in clinical settings, for drug discovery screening, and for monitoring drug efficacy and toxicity. The current blood donation system for transfusion is incapable of providing enough granulocytes for patients with life-threatening neutropenia, although granulocyte transfusion could have a potentially significant benefit for a certain population of severely neutropenic patients.[11,12] Given the large amount of neutrophils required for transfusion,[13] hESC-derived neutrophils might be a unique solution for this treatment demand. Therefore, the development of a highly effective method of neutrophil differentiation from hESCs is an important step for both clinical application of hESCs and granulocyte transfusion medicine.

The lack of an effective method for obtaining hESC-derived neutrophils with purity sufficient for functional analysis, however, has hampered progress in this field. Once neutrophils with a high purity can be generated from hESCs, it will be important to compare their activities with those of neutrophils produced in vivo, particularly given the fact that hESCs rarely give rise to hematopoietic stem cells in vitro,[14] and thus, that hESC-derived neutrophils might not be a progeny of hematopoietic stem cells. Here, we developed an effective method of deriving mature neutrophils from hESCs through EB formation and subsequent coculture with OP9, and analyzed their morphologic and phenotypic characteristics. We then performed functional analyses of hESC-derived neutrophils in vitro, focusing on superoxide production, phagocytosis, bactericidal activity, and chemotaxis, in comparison with peripheral blood neutrophils (PB-Neu's) obtained from healthy subjects.

Methods

Human ES cell culture and EB formation

In all experiments using hESCs, we used KhES-3[15] cells (a kind gift from Dr Nakatsuji; Kyoto University, Kyoto, Japan), which were maintained as previously described.[16] Briefly, KhES-3 colonies were cultured on irradiated mouse embryonic fibroblasts in Dulbecco modified Eagle medium/F12 (Invitrogen, Carlsbad, CA) supplemented with 20% KNOCKOUT serum

Submitted May 31, 2008; accepted March 5, 2009. Prepublished online as *Blood* First Edition paper, March 25, 2009; DOI 10.1182/blood-2008-06-160838.

An Inside *Blood* analysis of this article appears at the front of this issue.

The publication costs of this article were defrayed in part by page charge payment. Therefore, and solely to indicate this fact, this article is hereby marked "advertisement" in accordance with 18 USC section 1734.